Electronic Supplementary Material (ESI) for Physical Chemistry Chemical Physics.

Experimental and theoretical study on the impact of a nitrate group on the chemistry of alkoxy radicals
— Supporting information —

A. Novelli, C. Cho, H. Fuchs, A. Hofzumahaus, F. Rohrer, R. Tillmann,
A. Kiendler-Scharr, A. Wahner, L. Vereecken

Table of Contents

A. Updating the ozonolysis schemes in the MCM

A.1 Ethene

The mechanism for the ozonolysis has been a subject of debate, in particular the pathways leading to the OH radical. Up until recently, it was proposed to be formed through the dioxirane channel, which forms a hot acid, HCOOH*, which can decompose to OH + HCO. However, from pyrolysis experiments and theoretical data, it is known that unimolecular decomposition of formic acid preferentially proceeds through the H_2 + CO_2 and H_2O + CO channels, with very similar barriers of 60-70 kcal mol^{-1}.[1–6] While the hot acid, through its chemical activation, can have a much larger energy content than achieved in the pyrolysis experiments, formation of free OH radicals (OH + HCO) or free H-atoms (CO_2 + 2 H) require significantly more energy, 107 and 98 kcal mol^{-1} respectively,[7] and is thus unlikely to contribute more than a few percent, *i.e.* unlikely to explain the experimentally observed yield of 17% OH. Other decomposition channels include H + HOCO (97 kcal mol^{-1}) and H + HC(=O)O (110 kcal mol^{-1}).[7] The direct OH-forming channel from CH_2OO^*, i.e. the 1,3-H-shift forming HCO + OH, has a much higher barrier than the dioxirane channel and can not compete effectively, contributing a few % of OH at most. Theoretical work by Stone et al.[8] and Peltola et al.[4] also found a low OH yield from stabilized CH_2OO; these studies do not include all exit channels that are energetically and/or entropically more favorable than OH formation, and their OH yield is thus likely an upper limit.

The recent theoretical work by Pfeifle et al.[9] shows an alternative mechanism for OH formation, following a non-Criegee pathway for the decomposition of the primary ozonide, forming highly energized $HC(=O)CH_2OOH$ which can be expected to decompose fully to HCO + CH_2O + OH, owing to the weak peroxide bond followed by rapid decomposition of the β-oxo-alkoxy radical.[9,10] The theoretically derived yield through the $HC(=O)CH_2OOH$ channel is ~12 %, close to the observed OH yield.

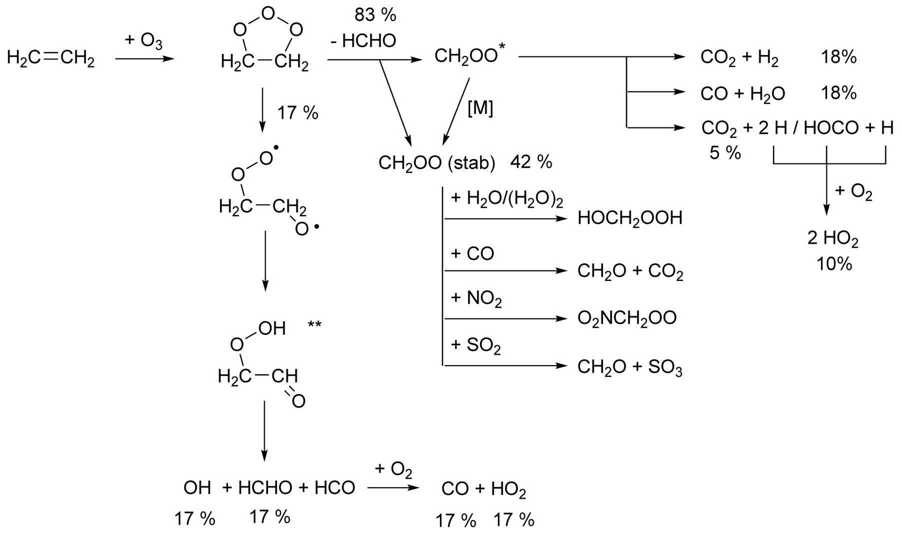

Figure S1: Ozonolysis reaction scheme for ethene

From an energetic point of view, and accounting for the experimental pyrolysis data for formic acid, it is thus probable that the OH formed in the ozonolysis of C_2H_4 is (near-)exclusively due to the $HC(=O)CH_2OOH$ channel, with the energized CH_2OO^* CI decomposing mainly to CO_2 + H_2 and CO + H_2O in near equal amounts, perhaps with a small yield of CO_2 + 2 H atoms or HOCO + H (the third and fourth most favorable hot acid decomposition channel), and little to no OH. Likewise, we assume that the 1,3-H-shift has a minor impact due to its high energy barrier. Accepting the recommended SCI yield of

42%, the resulting mechanism also recovers the currently recommended yields for CO_2, (23%), CO (35%), HO_2 (27%) and H_2O (18%).[11] Following are the ozonolysis reactions as implemented within the model following the nomenclature in use in the MCMv3.3.1, were we assume that free H-atoms, HOCO, and HCO all react with O_2 forming HO_2.:

k[C2H4 + O3 --> OH + HCHO + CO + HO2]=CONST(9.1D-15*EXP(-2580/(T))*0.17)
k[C2H4 + O3 --> HCHO + CH2OO]=CONST(9.1D-15*EXP(-2580/(T))*0.42)
k[C2H4 + O3 --> HCHO + CO2 + H2]=CONST(9.1D-15*EXP(-2580/(T))*0.18)
k[C2H4 + O3 --> HCHO + CO + H2O]=CONST(9.1D-15*EXP(-2580/(T))*0.18)
k[C2H4 + O3 --> HCHO + CO2 + HO2 + HO2]=CONST(9.1D-15*EXP(-2580/(T))*0.05)

At this time, it is unclear how important the carbonyl-hydroperoxide channel by Pfeifle et al.[9] is for other alkenes. As it requires the H-migration of one of the vinylic hydrogens, it will be absent in tetra-substituted alkenes such as 2,3-dimethyl-2-butene. For partially substituted alkenes it would decrease in importance as a function of the decreasing number of H-atoms on the double-bonded carbons, but the energetic and entropic features of these reactions are not known. Given that substituted alkenes tend to have a much larger OH yield, with most of the OH formed through the vinylhydroperoxide channel in *syn*-substituted CI, we will at this time not consider this reaction in the ozonolysis of substituted alkenes.

The stabilized H_2COO SCI has a fairly slow unimolecular reaction with $k(298\ K) < 0.5\ s^{-1}$,[8,12] and will be scavenged by CO, NO_2 or other co-reactants in our experiments (see below), with a total pseudo-first order rate coefficient exceeding $5\ s^{-1}$.

A.2 Propene

Based on the available experimental data we adopt as a 62:38 ratio for the branching ratio of the decomposition of the primary ozonide to CH_3CHOO + HCHO and CH_2OO + CH_3CHO.[11,13,14] The results by Newland et al.[14] show a total SCI yield of 0.34, within the range from 0.25 to 0.44 set by earlier data.[13,15] Of the CH_2OO formed, 60 % is stabilized as measured by Newland et al.,[14] leading to an overall yield of stabilized CH_2OO of 23%. The remainder of the SCI, 11%, is stabilized CH_3CHOO. The reactions of these SCI are as for ethene and cis-2-butene, i.e. CH_2OO is scavenged while CH_3CHOO decays unimolecularly. *Syn*-CH_3CHOO is assumed to be the only source of OH, which was measured with a yield of 34%.[11,16] All *syn*-CH_3CHOO, activated or stabilized, is expected to convert to OH + O=$CHCH_2$, so we then speciate CH_3CHOO as 55% *syn*, 45% *anti*. The fate of *anti*-CH_3CHOO is assumed to be identical to that in *cis*-2-butene, i.e. forming a 2:1:1 ratio of CH_4, CH_3OH, and HO_2, with a small 2 % yield of stabilized acetic acid.

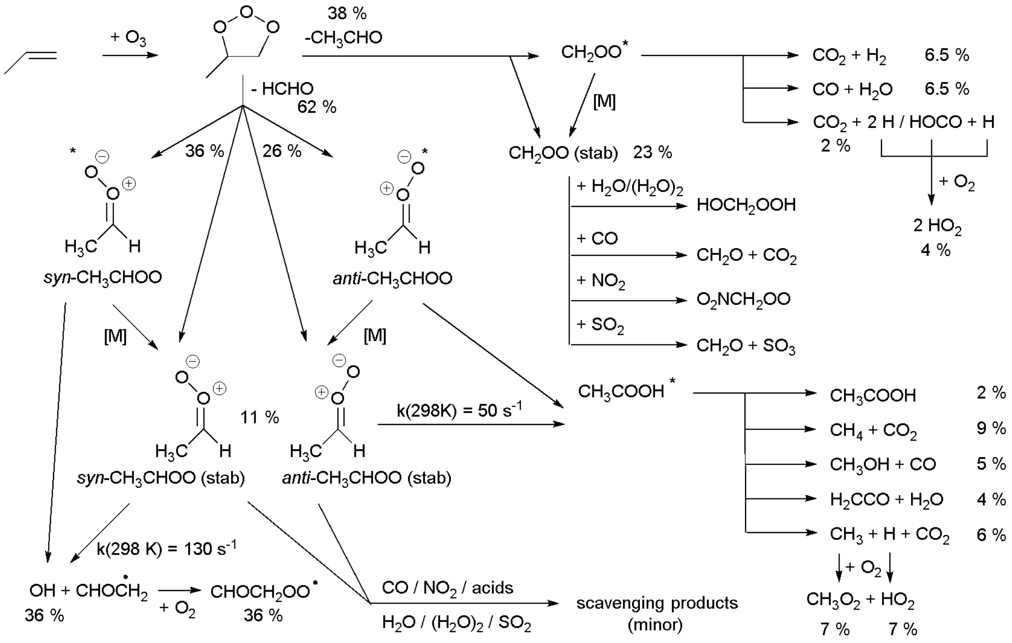

Figure S2: Ozonolysis reaction scheme for propene

Following are the ozonolysis reactions as implemented within the model following the nomenclature in use in the MCMv3.3.1:

k[C3H6 + O3 --> CH3CHO + CH2OO]=CONST(5.5D-15*EXP(-1880/(T))*0.23)
k[C3H6 + O3 --> CH3CHO + CO2 + H2]=CONST(5.5D-15*EXP(-1880/(T))*0.065)
k[C3H6 + O3 --> CH3CHO + CO + H2O]=CONST(5.5D-15*EXP(-1880/(T))*0.065)
k[C3H6 + O3 --> CH3CHO + HO2 + HO2 + CO2]=CONST(5.5D-15*EXP(-1880/(T))*0.02)
k[C3H6 + O3 --> HCHO + OH + HCOCH2O2]=CONST(5.5D-15*EXP(-1880/(T))*0.36)
k[C3H6 + O3 --> CH3CO2H]=CONST(5.5D-15*EXP(-1880/(T))*0.02)
k[C3H6 + O3 --> HCHO + CH4 + CO2]=CONST(5.5D-15*EXP(-1880/(T))*0.12)
k[C3H6 + O3 --> HCHO + CH3OH + CO]=CONST(5.5D-15*EXP(-1880/(T))*0.06)
k[C3H6 + O3 --> HCHO + CH3O2 + HO2 + CO2]=CONST(5.5D-15*EXP(-1880/(T))*0.06)

A.3 Cis-2-butene

The ozonolysis of cis-2-butene always yields acetaldehyde + CH_3CHOO. The branching ratio between the *syn*-CH_3CHOO and *anti*-CH_3CHOO products we adopt is based on the assumption that most of the OH formed comes from the dominant vinylhydroperoxide decomposition path for *syn*-CH_3CHOO, both as chemically activated CI or as SCI; the thermal rate coefficient at 298 K is about 130 s^{-1}.[12,17–20] The literature OH yield of 37 %[11,16,21] then requires 63 % *anti*-CH_3CHO, a ratio in agreement with the results by Rathman et al.[22] We assume that *anti*-CH_3CHO, decaying unimolecularly through the dioxirane channel, yields CH_4, CH_3OH, CO_2, and HO_2 in a 2:1:1 ratio, close to the recommended ratios,[11] with a small yield of 3 % stabilized acetic acid as measured by Orzechowska and Paulson.[23] As the base MCM v3.3.1 model does not include the chemistry of ketene, $H_2C{=}C{=}O$, this product is omitted, despite that ketene formation is known to be a main channel in pyrolysis of alkylcarboxylic acids.[24–27] Note that the experimental product data does not yield a closed carbon balance. The thermal unimolecular rate for *anti*-CH_3CHO was calculated at 50 s^{-1},[12] indicating that scavenging of this SCI is unlikely, which agrees with the minor impact of high water concentrations on the yield of acetic acid formed from this CI.[23]

Berndt et al.[28] measured a stabilization fraction of 0.53 ± 0.24 % for *trans*-2-butene; for *cis*-2-butene it should be in the same order of magnitude despite the slightly higher ozonolysis reaction exoergicity. Campos-Pineda and Zhang[29] infer from their lower-pressure SCI yield for *cis*-2-butene that the SCI yield might be above 0.20. The IUPAC recommended value is 38% [11]. In our reaction system, with low water content and low co-reactant concentrations, any stabilized CI are expected to decay mostly by unimolecular reaction. The total loss by the most relevant co-reactants, NO_2 and CO, remains below 10 s^{-1} . As such, we are not sensitive to the stabilization yield and the speciation of the SCI.

Following are the ozonolysis reactions as implemented within the model following the nomenclature in use in the MCMv3.3.1

k[CBUT2ENE + O3 --> OH + HCOCH2O2 + CH3CHO]=CONST(3.22D-15*EXP(-968/(T))*0.36)
k[CBUT2ENE + O3 --> CH4 + CO2 + CH3CHO]=CONST(3.22D-15*EXP(-968/(T))*0.31)
k[CBUT2ENE + O3 --> CH3O2 + HO2 + CO2 + CH3CHO]=CONST(3.22D-15*EXP(-968/(T))*0.15)
k[CBUT2ENE + O3 --> CH3OH + H2O + CO + CH3CHO]=CONST(3.22D-15*EXP(-968/(T))*0.15)
k[CBUT2ENE + O3 --> CH3CO2H]=CONST(3.22D-15*EXP(-968/(T))*0.03)

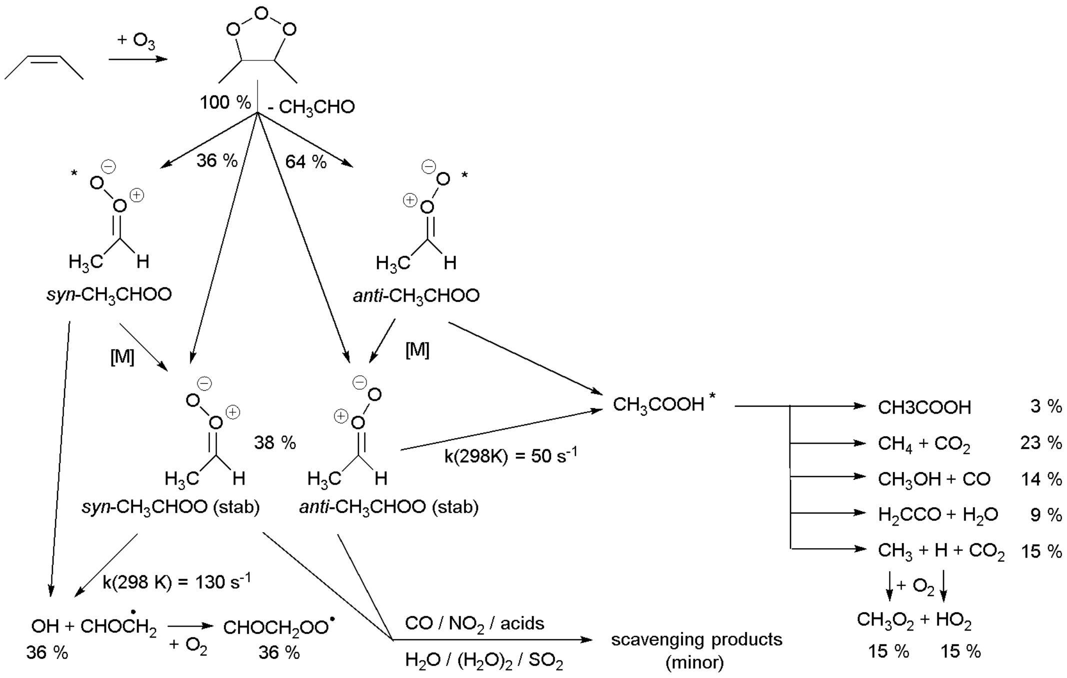

Figure S3: Ozonolysis reaction scheme for *cis*-2-butene

A.4 2,3-dimethyl-2-butene

The ozonolysis of 2,3-dimethyl-2-butene can yield only one CI, $(CH_3)_2COO$, which has been measured and calculated to decompose quickly through the vinylhydroperoxide channel, thus yielding ~100% OH.[12,30–32] Measurements of other products, such as acids,[23] indicates that these are secondary products formed in the subsequent chemistry. The chemistry in models M0 and M1 is not changed from the MCM model v3.3.1.

A.5 1-pentene

For 1-pentene, we assume the contribution of the HCHO-forming channel (55%), and the total yield of SCI (47%), is intermediate between that of 2-propene and 2-heptene[14] with the stabilization of the CH_2OO CI (60%) likewise similar to those two cases. The OH yield, 32%, is assumed to be similar to that of propene and 1-butene.[11] For excited CH_2OO, we assume the same chemistry as for ethene, whereas the stabilized CH_2OO is scavenged in our experiments. As their CH_3CHOO-equivalents, *syn*-C_3H_7CHOO is expected to decompose for 100% to OH + butanal-peroxy through the VHP channel, whereas for *anti*-C_3H_7CHOO, reacting through the dioxirane channel to a hot acid, is assigned products in similar ratios as for propene and 2-butene, i.e. a 2:1:1 ratio of $C_3H_8 + CO_2$, $C_3H_7OH + H_2O + CO$, and $C_3H_7 + H + CO_2$, though we assign a yield of 5 % stabilized butanoic acid, intermediate the measured acid yields of propene (3%) and 1-hexene (8%).[23,33]

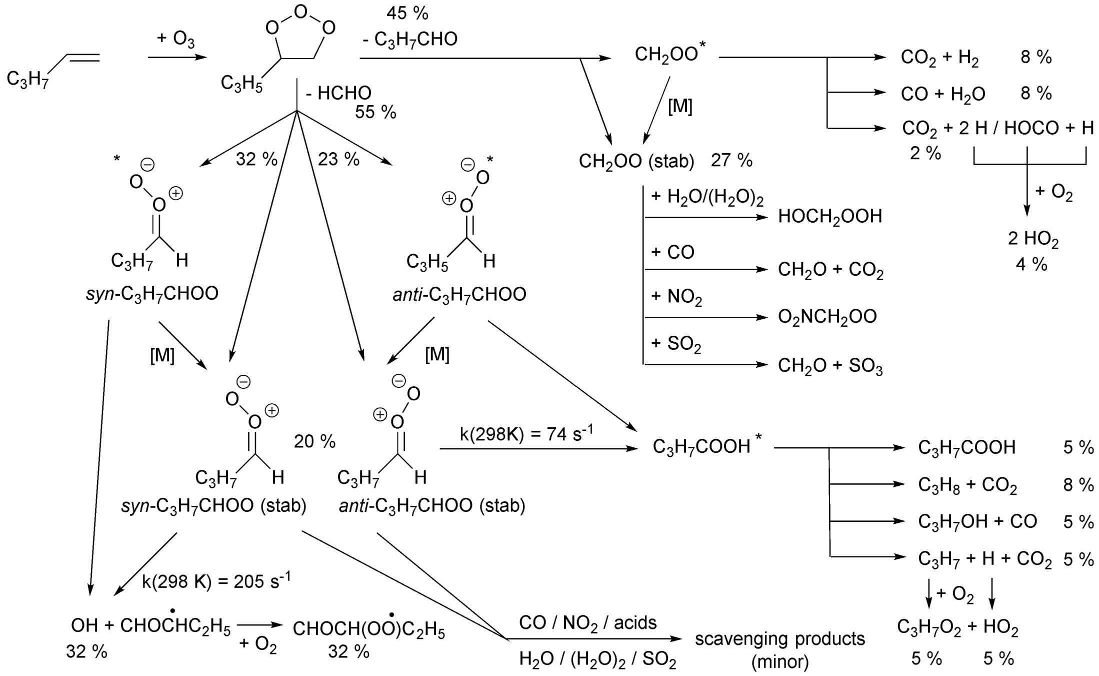

Figure S4: Ozonolysis reaction scheme for 1-pentene

Following are the ozonolysis reactions as implemented within the model following the nomenclature in use in the MCMv3.3.1:

k[PENT1ENE + O3 --> C3H7CHO + CH2OO]=CONST(1.00D-17*0.27)
k[PENT1ENE + O3 --> C3H7CHO + CO2 + H2]=CONST(1.00D-17*0.08)
k[PENT1ENE + O3 --> C3H7CHO + CO + H2O]=CONST(1.00D-17*0.08)
k[PENT1ENE + O3 --> C3H7CHO + CO2 + HO2 + HO2]=CONST(1.00D-17*0.02)
k[PENT1ENE + O3 --> HCHO + OH + BUTALAO2]=CONST(1.00D-17*0.32)
k[PENT1ENE + O3 --> BUTACID]=CONST(1.00D-17*0.05)
k[PENT1ENE + O3 --> HCHO + C3H8 + CO2]=CONST(1.00D-17*0.08)
k[PENT1ENE + O3 --> HCHO + NPROPOL + CO]=CONST(1.00D-17*0.05)
k[PENT1ENE + O3 --> HCHO + NC3H7O2 + HO2 + CO]=CONST(1.00D-17*0.05)

A.6 2-hexene

For 2-hexene, we adopt the following scheme, by analogy of the previous schemes.

Following are the ozonolysis reactions as implemented within the model following the nomenclature in use in the MCMv3.3.1:

k[THEX2ENE + O3 --> C3H7CHO + OH + HCOCH2O2]=CONST(1.60D-16*0.18)
k[THEX2ENE + O3 --> C3H7CHO + CH4 + CO2]=CONST(1.60D-16*0.16)
k[THEX2ENE + O3 --> C3H7CHO + CH3OH + H2O + CO]=CONST(1.60D-16*0.08)
k[THEX2ENE + O3 --> C3H7CHO + CH3O2 + HO2 + CO]=CONST(1.60D-16*0.08)
k[THEX2ENE + O3 --> CH3CHO + OH + BUTALAO2]=CONST(1.60D-16*0.3) ;0.3
k[THEX2ENE + O3 --> BUTACID]=CONST(1.60D-16*0.06)
k[THEX2ENE + O3 --> CH3CHO + C3H8 + CO2]=CONST(1.60D-16*0.08)
k[THEX2ENE + O3 --> CH3CHO + NPROPOL + CO]=CONST(1.60D-16*0.03) ; 0.03
k[THEX2ENE + O3 --> CH3CHO + NC3H7O2 + HO2 + CO]=CONST(1.60D-16*0.03)

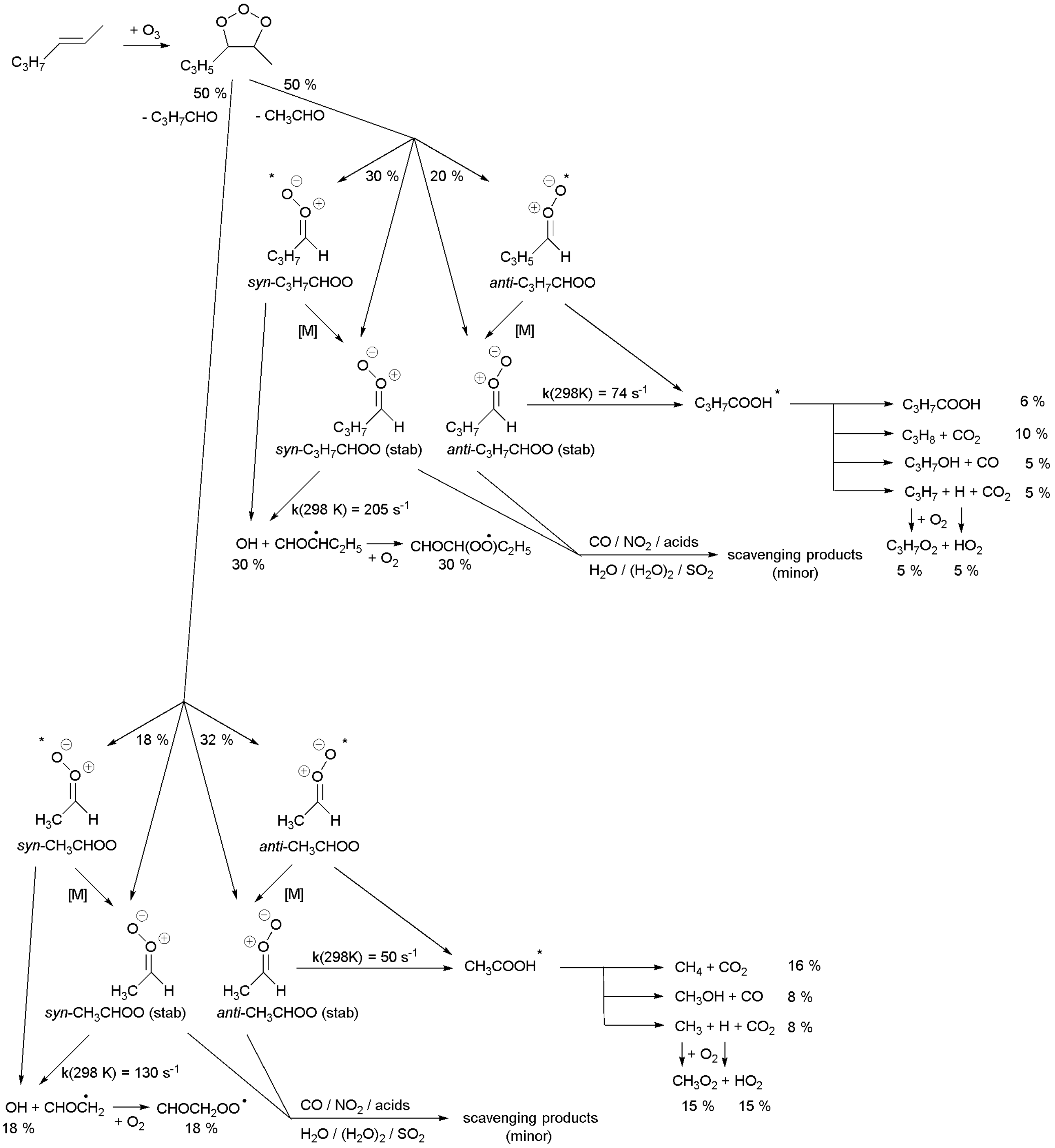

Figure S5: Ozonolysis reaction scheme for trans-2-hexene

A.7 SCI bimolecular reactions

In our reaction conditions, only two CI scavenging reactions are of potential importance:

$R_1R_2COO + NO_2 \rightarrow R_1R_2C(NO_2)OO^{\bullet}$ Vereecken and Nguyen,[34] Caravan et al.[35]

$R_1R_2COO + CO \rightarrow R_1R_2C{=}O + CO_2$ Vereecken et al.,[36] Kumar et al.[37,38]

We adopt the following rate coefficients (cm^3 $molecule^{-1}$ s^{-1}) for bimolecular reaction of CI:

SCI	CO	NO_2
CH_2OO	1×10^{-15}	3×10^{-12}
syn-CH_3CHOO	1×10^{-15}	2×10^{-12}
anti-CH_3CHOO	1×10^{-15}	2×10^{-12}
$(CH_3)_2COO$	1×10^{-15}	2.1×10^{-12}
syn-RCH_2CHOO	1×10^{-15}	2×10^{-12}
anti-RCH_2CHOO	1×10^{-15}	2×10^{-12}

With the rate coefficients listed above, the pseudo-first order rate coefficients are ~3 s^{-1} for the reaction with NO_2, and ~5 s^{-1} with CO. The scavenging reactions can then be neglected compared to the unimolecular reactions of the SCI, ≥ 50 s^{-1}, except for CH_2OO which decomposes umimolecularly with a rate < 1 s^{-1}.[12] Other scavenging agents, including NO_3, are even less effective due to their lower concentrations, and are not considered explicitly.

A.8 Updating SCI-derived alkylperoxy radical chemistry in the MCM

For the peroxy radicals formed in the reaction of SCI + NO_2, we adopt the following rate coefficients, estimated using the recent work by Jenkin et al.[39] With R_1 = H, CH_3, *n*-C_4H_9:

$R_1CH(NO_2)OO^{\bullet} + NO \rightarrow R_1CH(NO_2)O^{\bullet} + NO_2$ $k(T) = 2.7\times10^{-12}\exp(360K/T)$ cm^3 $molecule^{-1}$ s^{-1}
$H_2C(NO_2)OO^{\bullet} + HO_2 \rightarrow R_1CH(NO_2)OOH + O_2$ $k(T) = 1.7\times10^{-13}\exp(1300K/T)$ cm^3 $molecule^{-1}$ s^{-1}
$CH_3CH(NO_2)OO^{\bullet} + HO_2 \rightarrow R_1CH(NO_2)OOH + O_2$ $k(T) = 1.9\times10^{-13}\exp(1300K/T)$ cm^3 $molecule^{-1}$ s^{-1}
$C_4H_9CH(NO_2)OO^{\bullet} + HO_2 \rightarrow R_1CH(NO_2)OOH + O_2$ $k(T) = 2.4\times10^{-13}\exp(1300K/T)$ cm^3 $molecule^{-1}$ s^{-1}
$R_1CH(NO_2)OO^{\bullet} + RO_2 \rightarrow R_1CH(NO_2)O^{\bullet}$ $k(T) = 0.6 \times 2\times10^{-12}$ cm^3 $molecule^{-1}$ s^{-1}
$\rightarrow R_1CH(NO_2)OH$ $k(T) = 0.2 \times 2\times10^{-12}$ cm^3 $molecule^{-1}$ s^{-1}
$\rightarrow R_1C(NO_2){=}O$ $k(T) = 0.2 \times 2\times10^{-12}$ cm^3 $molecule^{-1}$ s^{-1}

The pseudo-first order rate coefficient for the reaction of peroxy radicals with NO_3 is $\leq 10^{-4}$ s^{-1}, and can be neglected in our experimental conditions:

$RO_2 + NO_3 \rightarrow RO + NO_2 + O_2$ $k(T) = 8.9\times10^{-12}\exp(-390K/T)$ cm^3 $molecule^{-1}$ s^{-1} [39]

As only the CH_2OO SCI is non-negligibly scavenged by NO_2, we implemented only the $CH_2(NO_2)OO^{\bullet}$ chemistry in our model.

A.9 Updating SCI-derived alkoxy radical chemistry in the MCM

The alkoxy radicals formed from the RO_2 radicals created in the scavenging of CI by NO_2 decompose rapidly to the carbonyl compound, regenerating NO_2.[34] With R_1 = H, CH_3, *n*-C_4H_9:

$R_1CH(NO_2)O^{\bullet} \rightarrow R_1CH{=}O + NO_2$ $k(298K) = 1.5\times10^{8}$ s^{-1}

As only the CH_2OO SCI is non-negligibly scavenged by NO_2, we implemented only the $CH_2(NO_2)O^{\bullet}$ decomposition.

A.10 Degradation scheme for ethanal-2-peroxy (HCOCH2O2) and butanal-2-peroxy (BUTALAO2)

The formation of OH radicals in the ozonolysis of alkenes typically occurs through the so-called vinyl-hydroperoxide (VHP) channel.[40,41] The Criegee intermediate (CI), be it thermalized or chemically excited, undergoes a 1,4-H-migration, forming a VHP that eliminates an OH radical, forming a vinoxy radical.

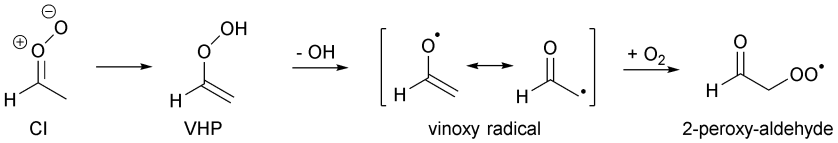

In atmospheric conditions, this vinoxy radical typically adds an O_2 molecule, forming a 2-peroxy-aldehyde or 2-peroxy-ketone, depending on the substitution on the alkene double bond. Despite the importance of this channel, the fate of these peroxyradicals has not been well-studied yet, and their complex atmospheric oxidation is often not correctly implemented in kinetic models. For aldehyde-2-peroxy radicals, 1,4-H-migration is likely to be an important loss process, as these reactions have been characterized as being among the fastest H-migrations of peroxy radicals, with a recent SAR by Vereecken and Nozière[42] predicting rate coefficients for this class exceeding 1 s^{-1}. The resulting 2-hydroperoxy-acyl radical can eliminate a CO molecule, forming an aldehyde and an OH radical as co-products, or can recombine with O_2 molecules forming a 2-OOH-acylperoxy radical. These radicals can also undergo very fast H-migrations, with rates exceeding 10^3 s^{-1},[42,43] forming 2-percarboxyl-peroxy radicals. In the high-NO conditions of the converter, these RO_2 radicals ultimately generate HO_2 radicals, after a series of oxidative steps.

For the alkenes studied in this work, the ozonolysis VHP channels produce ethanal-2-peroxy ($^{\bullet}OOCH_2CH{=}O$) and butanal-2-peroxy ($C_2H_5CH(OO^{\bullet})CH{=}O$) radicals. To characterize their atmospheric chemistry, and their behavior in the atmospheric chamber and the LIF converter, we have performed a set of quantum chemical calculations at the CCSD(T)/aug-cc-pVTZ// M06-2X-D3/aug-cc-pVTZ level of theory, combined with MC-TST kinetic rate predictions. The resulting kinetic data is tabulated below (see Table S1), and reaction schemes are shown below. For reactions where we do not provide direct theoretical kinetic data, literature structure activity relationships and explicit theoretical calculations for similar alkyl (R), alkoxy (RO) and alkylperoxy (RO_2) radical were used to obtain rate coefficients.[10,39,42–45] In the schemes below, dotted arrows indicate conversion of an RO_2 to an RO conversion through reaction with NO, NO_3, HO_2, or $R'O_2$; these reactions are not show explicitly in the reaction schemes except to highlight a specific rate coefficient or competition. In the converter, there is a high NO concentration, and conversion of RO_2 to RO radicals is fast. Also indicated is PAN formation for acylperoxy radicals. Our calculations find no impact of the –OOH substituent on the stability of the PAN, with a stabilization energy of 27.6 kcal mol^{-1}, identical to that found for peroxyacetylnitrate, 27.7 kcal mol^{-1}. There is thus no indications that PAN formation would be more favorable for these oxygenated acylperoxy radicals.

Table S1: Theoretical rate predictions at the CCSD(T)/aug-cc-pVTZ//M06-2X-D3/aug-cc-pVTZ with MC-TST level of theory. Indicated are the ZPE-corrected barrier height (E_b, kcal mol^{-1}), the 298 K rate coefficient (k(298 K), s^{-1}), and the parameters for a Kooij expression $k(T) = A\times(T/K)^n\times\exp(-E_a/T)$ (A in s^{-1}, E_a in K).

Reaction	Mechanism	E_b	***k*(298 K)**	A	n	E_a
$^{\bullet}OOCH_2CH{=}O \rightarrow HOOCH_2C^{\bullet}{=}O$	1,4-H-migration	21.7	3.9×10^{-2}	2.07E-70	26.14	-2471
$HOOCH_2C^{\bullet}{=}O \rightarrow CO + HCHO + OH$	Fragmentation	10.7	2.9×10^{5}	2.27E+12	0.47	5529
$HOOCH_2C({=}O)OO^{\bullet} \rightarrow {}^{\bullet}OOCH_2C({=}O)OOH$	1,6-H-migration	19.6	8.1×10^{2}	2.94E-35	13.82	-2222
$^{\bullet}OOCH_2C({=}O)OOH \rightarrow HOOCH_2C({=}O)OO^{\bullet}$	1,6-H-migration	25.4	8.5×10^{-3}	2.98E-41	15.62	135
$^{\bullet}OCH_2C({=}O)OOH \rightarrow HCHO + CO_2 + OH$	Fragmentation	15.9	5.5×10^{0}	1.34E-03	5.55	6947
$^{\bullet}OCH_2C({=}O)OOH \rightarrow HOCH_2C({=}O)OO^{\bullet}$	1,5-H-migration	13.0	6.9×10^{3}	6.09E-42	17.30	-1546
$HOCH_2C({=}O)OO^{\bullet} \rightarrow {}^{\bullet}OCH_2C({=}O)OOH$	1,5-H-migration	25.0	1.4×10^{-5}	1.31E-38	16.18	4812
$HOCH_2C({=}O)OO^{\bullet} \rightarrow HCHO + CO + HO_2$	HO_2 elimination	39.3	1.8×10^{-16}	6.68E+08	1.44	19299
$C_2H_5CH(OO^{\bullet})CH{=}O \rightarrow C_2H_5CH(OOH)C^{\bullet}{=}O$	1,4-H-migration	21.0	2.5×10^{-1}	8.06E-66	24.86	-2052
$C_2H_5CH(OO^{\bullet})CH{=}O \rightarrow C^{\bullet}H_2CH_2CH(OOH)CH{=}O$	1,5-H-migration	23.6	4.3×10^{-5}	2.92E-21	10.17	6162
$C_2H_5CH(OOH)C^{\bullet}{=}O \rightarrow CO + HCHO + OH$	Fragmentation	9.3	3.3×10^{6}	3.97E+11	0.74	4737
$C_2H_5CH(OOH)C({=}O)OO^{\bullet} \rightarrow C_2H_5CH(OO^{\bullet})C({=}O)OOH$	1,6-H-migration	18.4	3.7×10^{2}	8.91E-38	14.57	-2456
$C_2H_5CH(OO^{\bullet})C({=}O)OOH \rightarrow C_2H_5CH(OOH)C({=}O)OO^{\bullet}$	1,6-H-migration	25.9	3.8×10^{-4}	7.16E-44	16.53	808

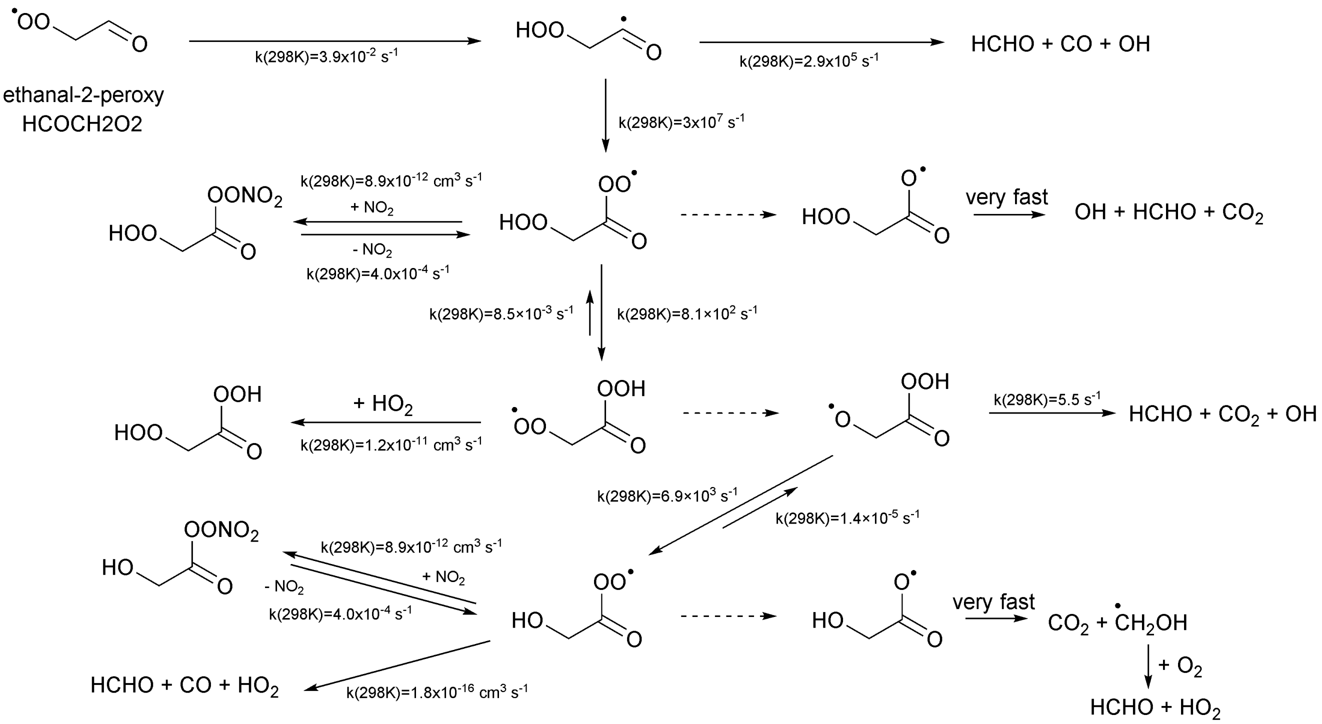

Figure S6: Reaction scheme for ethanal-2-peroxy radicals

Following are the reactions as implemented within the model following the nomenclature in use in the MCMv3.3.1:

```
; Minor pathways have been removed
; Variables for SAR by Jenkin et al., ACP, 2019
AlkNitrate5 = CONST(((2E-22*exp(5)*M)/(1+((2E-22*exp(5)*M)/(0.43*(T/300.)@(-8)))))*0.41@((1+
(log10((2E-22*exp(5)*M)/(0.43*(T/300.)@(-8))))@(2))@(-1)))
SARRO2HO2_5NOC = CONST(2.8E-13*exp(1300./T)*(1-exp(-0.23*5)))
; Chemistry complementing the chemistry in MCM v3.3.1
k[HCOCH2O2 --> COCH2OOH]=CONST(2.07E-70*T@(26.14)*EXP(2471./T))
k[COCH2OOH --> HCHO+CO+OH]=CONST(2.27E+12*T@(0.47)*EXP(-5529./T))
k[COCH2OOH + O2 --> HOOCH2CO3]=CONST(7.50D-12)
; acylperoxy radical chemistry
k[HOOCH2CO3 --> CO3HCH2O2]=CONST(2.94E-35*T@(13.82)*EXP(2222./T))
k[HOOCH2CO3+HO2 --> HO2CH2CO3H]=CONST(KAPHO2*0.41)
k[HOOCH2CO3+HO2 --> OH+HOOCH2CO2]=CONST(KAPHO2*0.44)
k[HOOCH2CO3+HO2 --> O3+HOOCH2CO2H]=CONST(KAPHO2*0.15)
k[HOOCH2CO3+NO3 --> OCOCH2OOH + NO2]=CONST(KRO2NO3*1.74)
k[HOOCH2CO3+RO2 --> HOOCH2CO2]=CONST(1.0D-11*0.7)
k[HOOCH2CO3+RO2 --> HOOCOCH2OOH]=CONST(1.0D-11*0.3)
k[HOOCH2CO3+NO --> HOOCH2CO2 + NO2]=CONST(KAPNO)
k[HOOCH2CO3+NO2 --> HOOCH2CO3NO2]=CONST(KFPAN)
k[HOOCH2CO3NO2 --> NO2 + HOOCH2CO3]=CONST(KBPAN)
k[HOOCH2CO2 --> CO2 + HCHO + OH]=CONST(KDEC)
; peracid-RO2 radical chemistry
k[CO3HCH2O2 --> HOOCH2CO3]=CONST(2.98E-41*T@(15.62)*EXP(-135./T))
k[CO3HCH2O2+HO2 --> HO2CH2CO3H]=CONST(SARRO2HO2_5NOC)
k[CO3HCH2O2+NO3 --> CO3HCH2O + NO2]=CONST(1.6E-11*EXP(-480./T))
k[CO3HCH2O2+RO2 --> CO3HCH2O]=CONST(1.0E-13*EXP(983./T)*0.6)
k[CO3HCH2O2+RO2 --> HCOCO3H]=CONST(1.0E-13*EXP(983./T)*0.2)
k[CO3HCH2O2+RO2 --> HOCH2CO3H]=CONST(1.0E-13*EXP(983./T)*0.2)
k[CO3HCH2O2+NO --> CO3HCH2O + NO2]=CONST(KRO2NO*(1-AlkNitrate5*0.3*0.65))
k[CO3HCH2O2+NO --> CO3HCH2NO3]=CONST(KRO2NO*AlkNitrate5*0.3*0.65)
; peracid-RO radical chemistry. Hydroxyacylperoxy product HOCH2CO3 is
; already in MCM v3.3.1
k[CO3HCH2O --> HO + CO2 + HCHO]=CONST(1.34E-03*T@(5.55)*EXP(-6947./T))
k[CO3HCH2O+O2 --> HCOCO3H + HO2]=CONST(KROPRIM)
k[CO3HCH2O --> HOCH2CO3]=CONST(1.31E-38*T@(16.18)*EXP(4812./T))
```

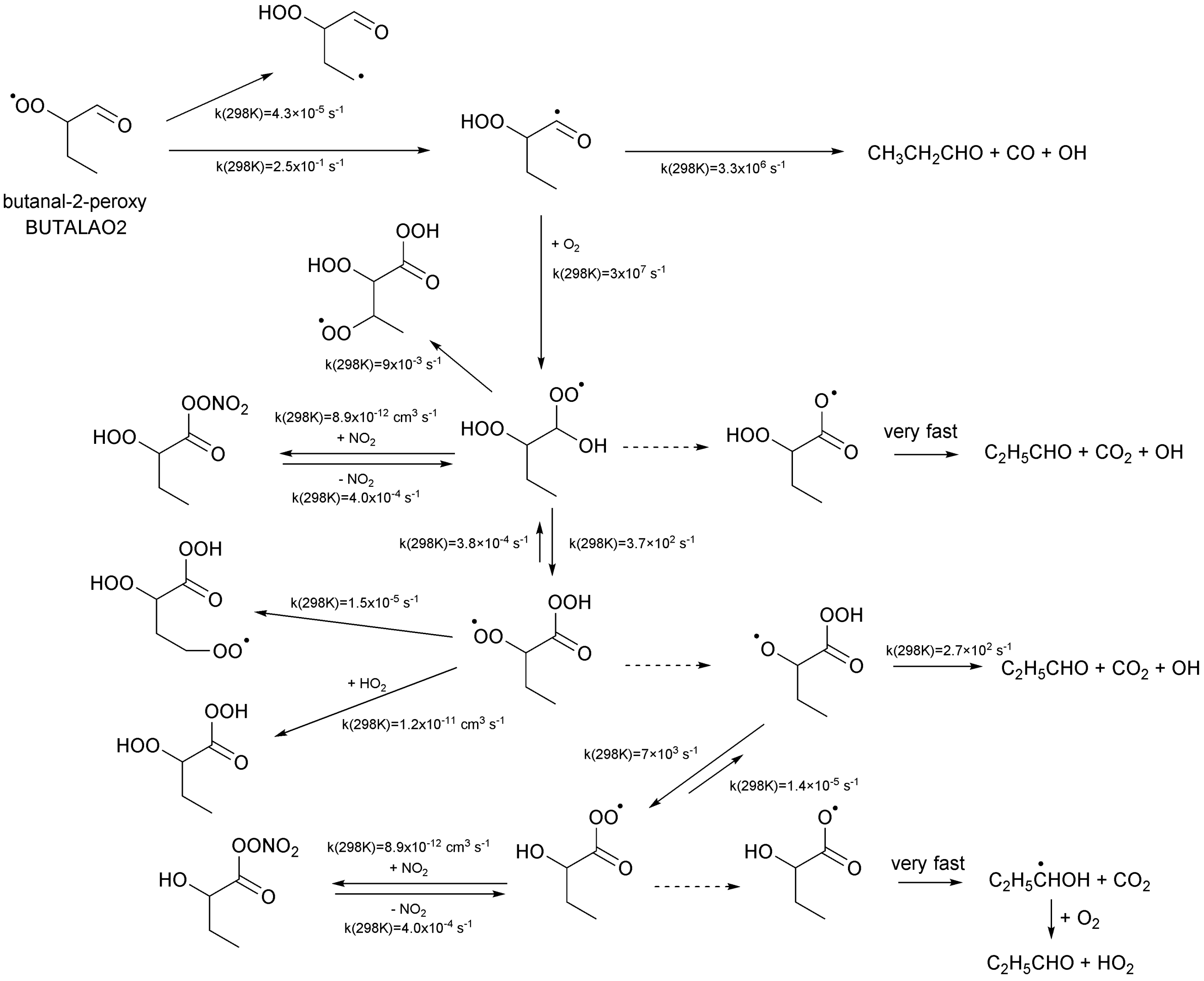

Figure S7: Reaction scheme for butanal-2-peroxy radicals

Following are the reactions as implemented within the model following the nomenclature in use in the MCMv3.3.1:

```
; Minor pathways have been removed
; Variables for SAR by Jenkin et al., ACP, 2019
AlkNitrate7=CONST(((2E-22*exp(7)*M)/(1+((2E-22*exp(7)*M)/(0.43*(T/300.)@(-8)))))*0.41@((1+
(log10((2E-22*exp(7)*M)/(0.43*(T/300.)@(-8))))@(2))@(-1)))
SARRO2HO2_7NOC=CONST(2.8E-13*exp(1300./T)*(1-exp(-0.23*7)))
; Chemistry complementing the chemistry in MCM v3.3.1
k[BUTALAO2 --> COCHOOHC2H5]=CONST(8.06E-66*T@(24.86)*EXP(2052/T))
k[COCHOOHC2H5 --> C2H5CHO+CO+OH]=CONST(3.97E+11*T@(0.74)*EXP(-4737/T))
k[COCHOOHC2H5 + O2 --> C2H5CHOOHCO3]=CONST(7.50D-12)
; acylperoxy radical chemistry
k[C2H5CHOOHCO3 --> C2H5CHO2CO3H]=CONST(8.91E-38*T@(14.57)*EXP(2456./T))
k[C2H5CHOOHCO3+HO2 --> C2H5CHOOHCO3H]=CONST(KAPHO2*0.41)
k[C2H5CHOOHCO3+HO2 --> OH+C2H5CHOOHCO2]=CONST(KAPHO2*0.44)
k[C2H5CHOOHCO3+HO2 --> O3+C2H5CHOOHCO2H]=CONST(KAPHO2*0.15)
k[C2H5CHOOHCO3+NO3 --> C2H5CHOOHCO2 + NO2]=CONST(KRO2NO3*1.74)
k[C2H5CHOOHCO3+RO2 --> C2H5CHOOHCO2]=CONST(1.0D-11*0.7)
k[C2H5CHOOHCO3+RO2 --> HOOCOCHOOH]=CONST(1.0D-11*0.3)
k[C2H5CHOOHCO3+NO --> C2H5CHOOHCO2 + NO2]=CONST(KAPNO)
k[C2H5CHOOHCO3+NO2 --> C2H5CHOOHCO3NO2]=CONST(KFPAN)
k[C2H5CHOOHCO3NO2 --> NO2 + C2H5CHOOHCO3]=CONST(KBPAN)
k[C2H5CHOOHCO2 --> CO2 + C2H5CHO + OH]=CONST(KDEC)
```

```
; peracid-RO2 radical chemistry
k[C2H5CHO2CO3H --> C2H5CHOOHCO3]=CONST(7.16E-44*T@(16.53)*EXP(-808./T))
k[C2H5CHO2CO3H+HO2 --> C2H5CHOOHCO3H]=CONST(SARRO2HO2_7NOC)
k[C2H5CHO2CO3H+NO3 --> C2H5CHOCO3H + NO2]=CONST(1.6E-11*EXP(-480./T))
k[C2H5CHO2CO3H+RO2 --> C2H5CHOCO3H]=CONST(1.0E-13*EXP(599./T)*0.6)
k[C2H5CHO2CO3H+RO2 --> C2H5COCO3H]=CONST(1.0E-13*EXP(599./T)*0.2)
k[C2H5CHO2CO3H+RO2 --> C2H5CHOHCO3H]=CONST(1.0E-13*EXP(599./T)*0.2)
k[C2H5CHO2CO3H+NO --> C2H5CHOCO3H + NO2]=CONST(KRO2NO*(1-AlkNitrate7*0.3*0.65))
k[C2H5CHO2CO3H+NO --> C2H5CHNO3CO3H]=CONST(KRO2NO*AlkNitrate7*0.3*0.65)
; peracid-RO radical chemistry. Base this on ethanal-2-peroxy, using SAR by
; Vereecken and Peeters (2009) to adjust decomposition rate. The hydroxy acylperoxy
; product HO3C3CO3  is already in the MCM
k[C2H5CHOCO3H --> HO + CO2 + C2H5CHO]=CONST(1.34E-03*T@(5.55)*EXP(-5789./T))
k[C2H5CHOCO3H+O2- -> HO3C3CO3 + HO2]=CONST(KROSEC)
k[C2H5CHOCO3H --> C2H5CHOHCO3]=CONST(1.31E-38*T@(16.18)*EXP(4812./T))
```

B. Additional calculations for 2-ONO$_2$-1-propoxy

Table S2 shows the large variation of barrier heights for decomposition in a simple reaction affected by the inhibiting effect of a β-ONO$_2$ group, as a function of the level of theory, i.e. the methodology or DFT functional used, as well as the basis set. The dependence of the energy on the methodology has already been documented in the supporting information by Vereecken and Peeters.[10] Despite the difference in energies across the base methodologies, the geometries appear consistent, with less than a kcal mol^{-1} on average difference in barrier height when performing higher-level single point CCSD(T) calculations. This indicates that the CCSD(T) energies used in this work are reliable.

Table S2: Barrier height E_b (kcal mol^{-1}) for the decomposition of $^{\bullet}OCH_2$-$CH(CH_3)ONO_2$ to $O{=}CH_2$ + $CH(CH_3){=}O$ + NO_2 at various levels of quantum chemical theory.

Geometry	***Base methodology energy***	**single point energy CCSD(T)/aug-cc-pVDZ**	**single point energy CCSD(T)/aug-cc-pVTZ**
B3LYP/6-31G(d,p)	12.93	14.33	12.89
B3LYP/aug-cc-pVTZ	9.39	14.68	13.37
MPWKCIS1K/6-31+(d,p)	19.73	14.12	
PMP2/6-31(d,p)	15.26	15.94	13.83
M06-2X/aug-cc-pVTZ	13.72	15.08	14.07
M06-2X-D3/aug-cc-pVTZ	13.71	15.08	14.07
CBS-QB3	11.78		

C. The stability of α-nitrite-substituted alkyl radicals

We performed CCSD(T)//aug-cc-pVTZ//M06-2X-D3/aug-cc-pVTZ calculations on the decomposition of $C^{\bullet}H_2ONO$ radicals, forming $CH_2{=}O$ + NO. At the M06-2X-D3 level of theory, this reaction shows a barrier to decomposition of only ~1 kcal mol^{-1}. The single-point energy calculations at the CCSD(T)/aug-cc-pVTZ level of theory lowered this barrier even further, to 0.05 kcal mol^{-1}, indicating that this reaction is spontaneous within the accuracy of the calculations.

$$C^{\bullet}H_2ONO \rightarrow CH_2{=}O + NO \qquad \text{(near-)barrierless}$$

As found in earlier work on –OOH, –OOR, and –ONO$_2$-substituted alkyl radicals,[46–48] it is anticipated that more substituted α-nitrite alkyl radicals have even lower barriers for elimination of NO, likely leading to the absence of an energy barrier for decomposition of such alkyl radicals. At atmospherically relevant temperatures, the decomposition of all α-nitrite alkyl radicals is expected to be very fast to instantaneous, precluding any other reactions including addition of O$_2$.

D. OH/NO$_3$-initiated degradation scheme for 1-pentene

The degradation scheme for the OH- and NO$_3$-initiated oxidation of 1-pentene was derived based on structure activity relationships for alkoxy (RO) and alkylperoxy (RO$_2$) radical isomerisation and decomposition,[10,42,44,47,48] as well as the explicit calculations report in this work. Most of the viable reaction channels were examined, and the dominant reaction channels (marked in blue) were implemented in the kinetic model. In the schemes, dotted arrows indicate conversion of an RO$_2$ to an RO conversion through reaction with NO, NO$_3$, HO$_2$, or R'O$_2$; these reactions are not indicated explicitly. The rate coefficients marked in blue are the dominant channels; only those reactions are implemented explicitly in the model.

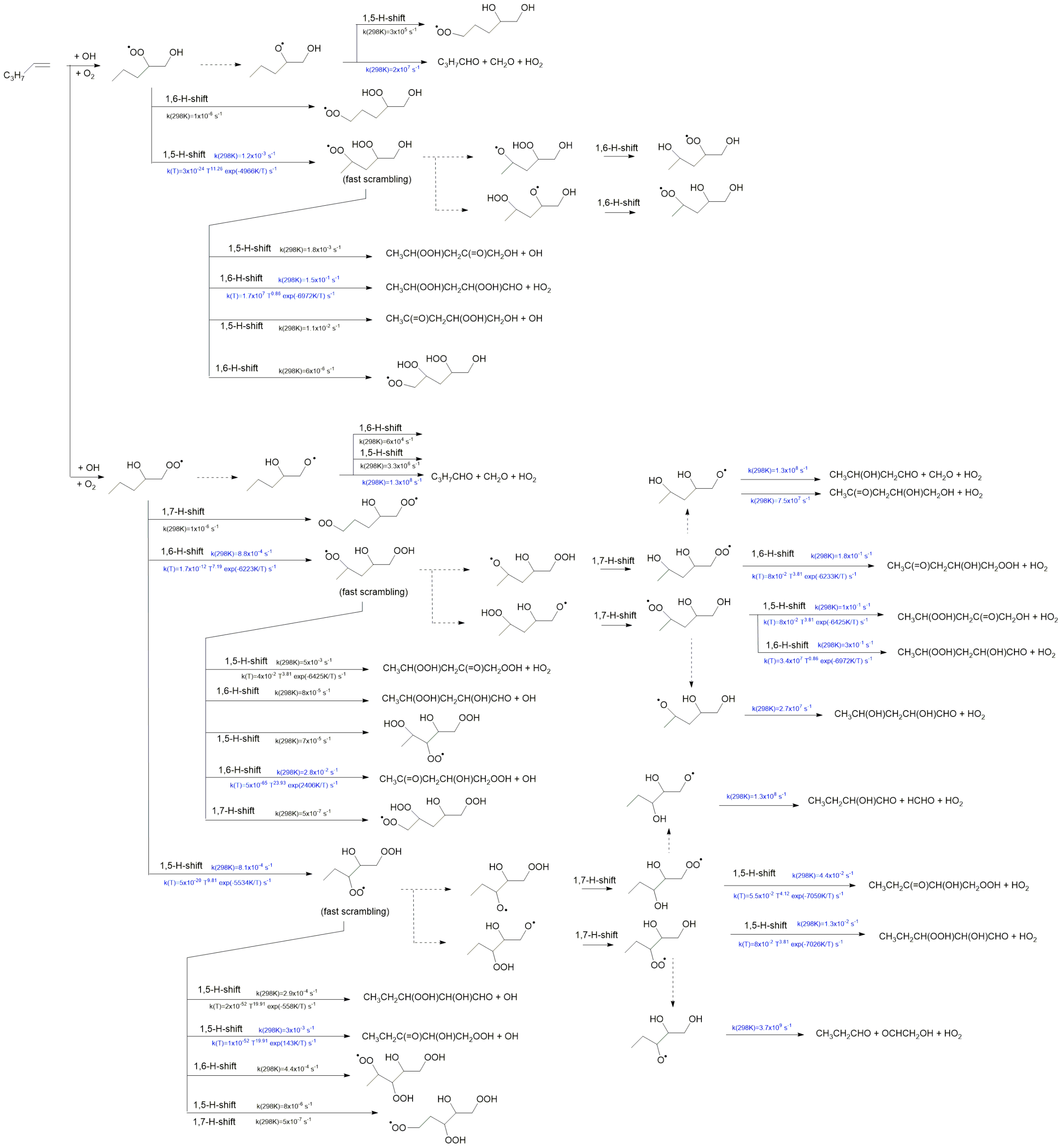

Figure S8: OH-initiated oxidation of 1-pentene

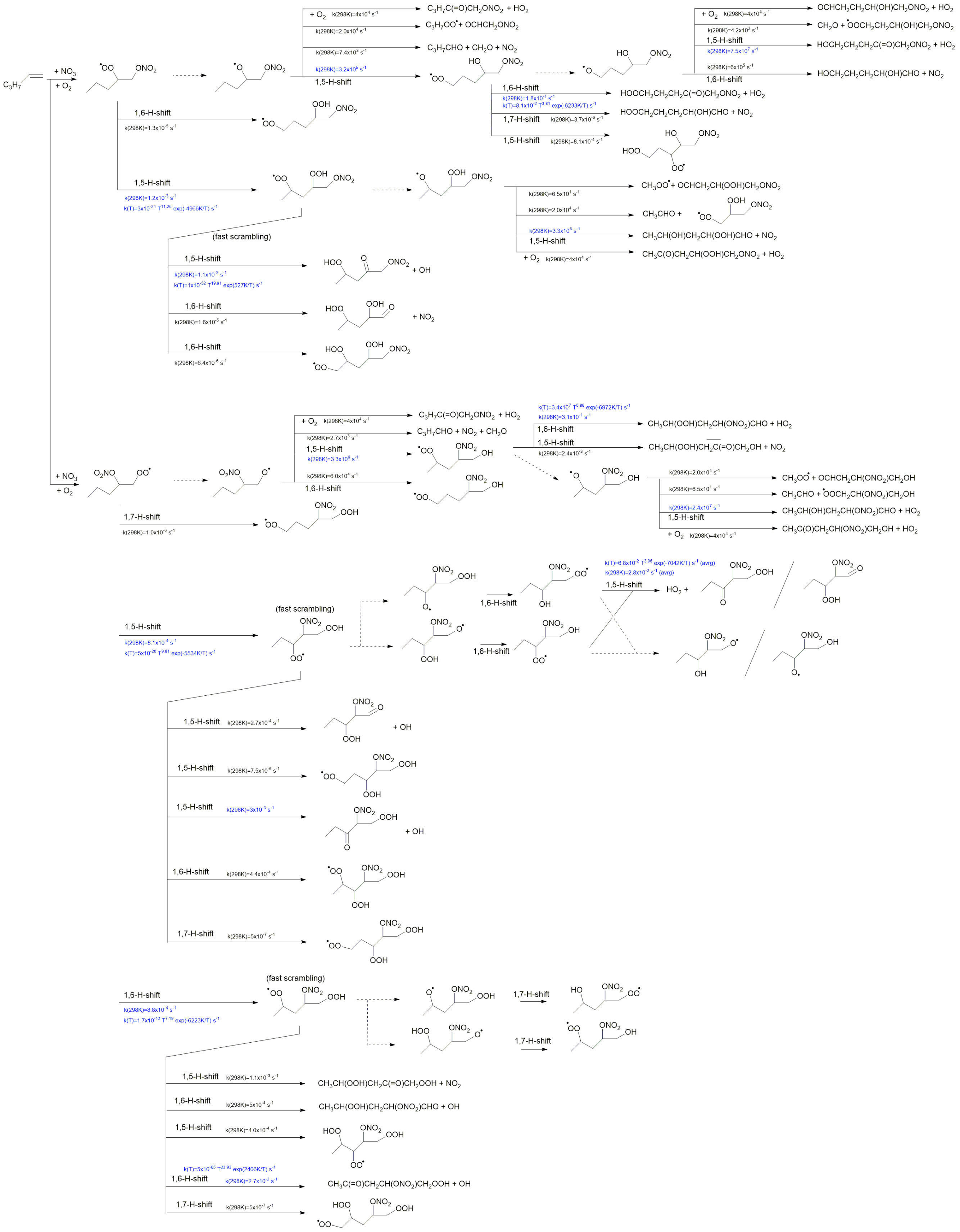

Figure S9: NO_3-initiated oxidation of 1-pentene

E. OH/NO$_3$-initiated degradation scheme for 2-hexene

The degradation scheme for the OH- and NO$_3$-initiated oxidation of 2-hexene was derived based on structure activity relationships for alkoxy (RO) and alkylperoxy (RO$_2$) radical isomerisation and decomposition[10,42,44,47,48] as well as the explicit calculations report in this work. Most of the viable reaction channels were examined, and the dominant reaction channels were implemented in the kinetic model. In the schemes below, dotted arrows indicate conversion of an RO$_2$ to an RO conversion through reaction with NO, NO$_3$, HO$_2$, or R'O$_2$; these reactions are not indicated explicitly. The rate coefficients marked in blue are the dominant channels; only those reactions are implemented explicitly in the model.

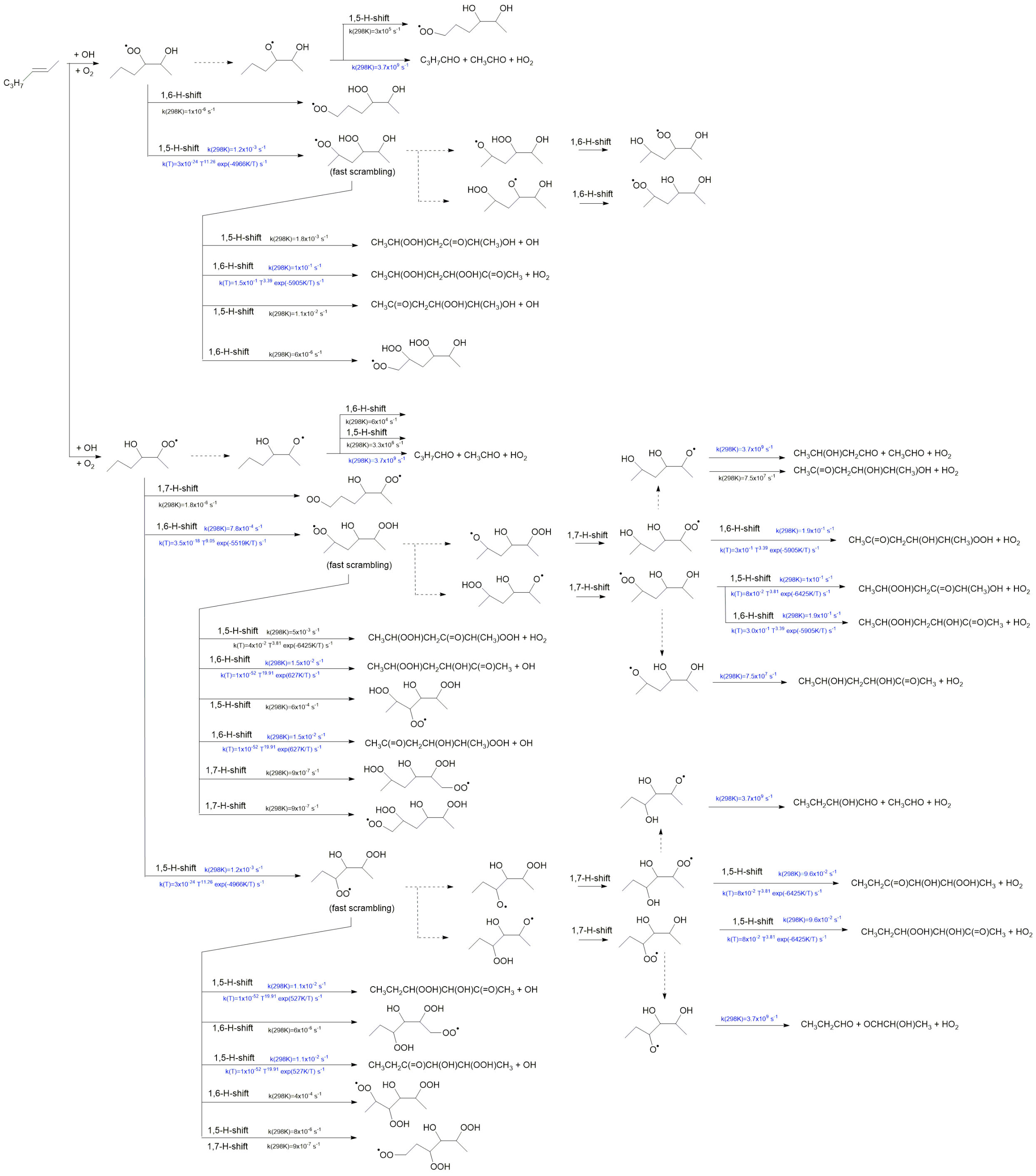

Figure S10: OH-initiated oxidation of trans-2-hexene

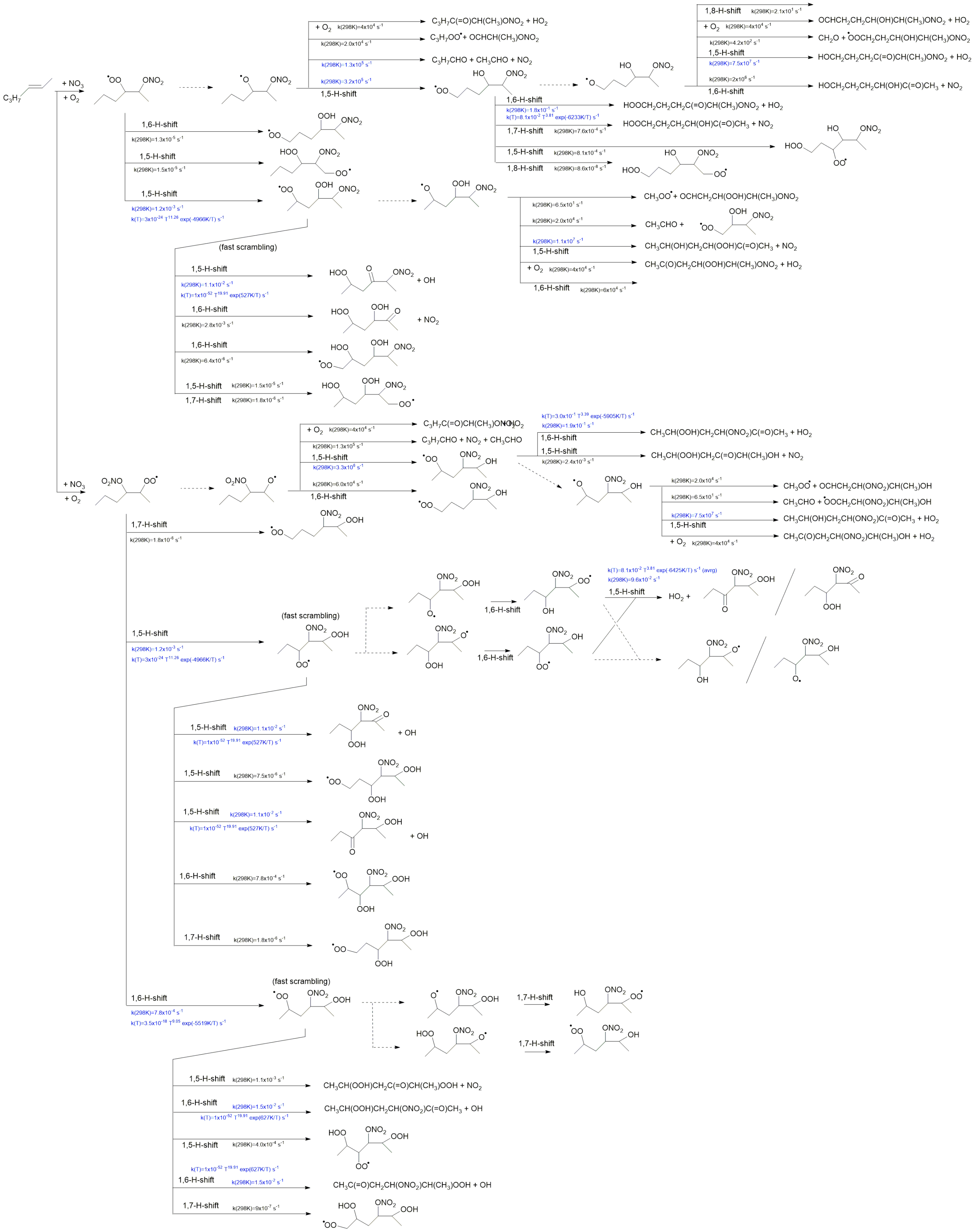

Figure S11: NO$_3$-initiated oxidation of trans-2-hexene

F. Time-dependent measured and modelled concentrations for all experiments

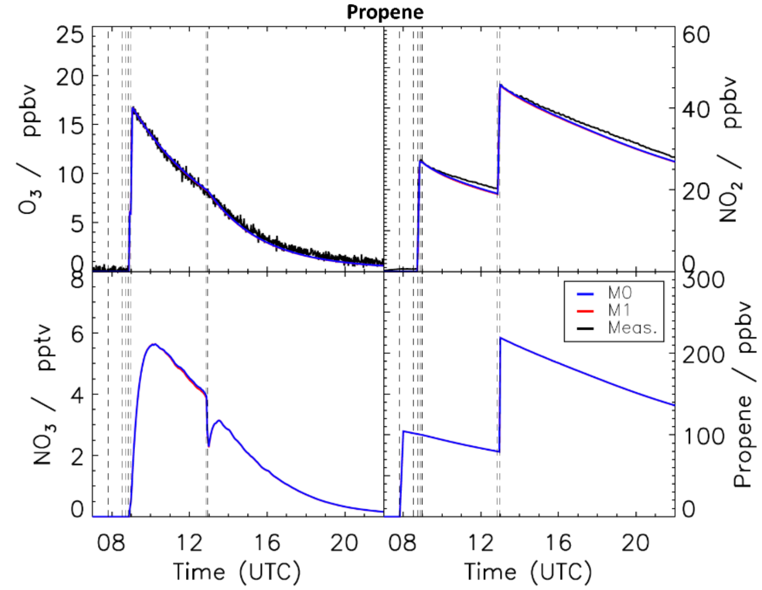

Figure S12: Comparison of modelled and measured trace gases for the propene experiment. For the NO_3 radical and propene only model results are shown. Vertical dashed lines indicate the times when different species where injected. No difference is observed when using the updated MCMv3.3.1 (M0) or a modified version which includes formation of alkoxy radical from the reaction between nitrate-RO_2 and HO_2 radicals (M1).

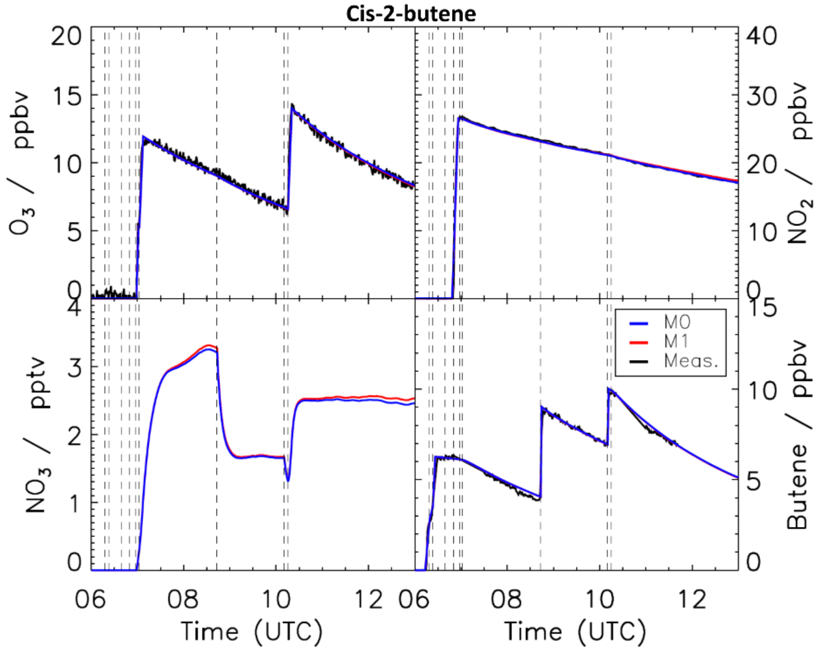

Figure S13: Comparison of modelled and measured trace gases for the *cis*-2-butene experiment. For the NO_3 radical only model results are shown. Vertical dashed lines indicate the times when different species where injected. No difference is observed when using the updated MCMv3.3.1 (M0) or a modified version which includes formation of alkoxy radical from the reaction between nitrate-RO_2 and HO_2 radicals (M1).

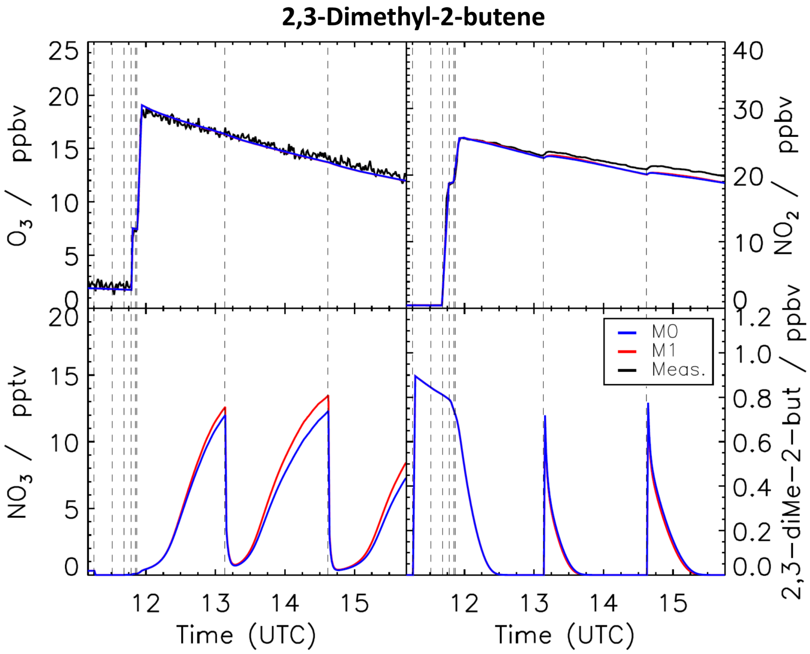

Figure S14: Comparison of modelled and measured trace gases for the 2,3-dimethyl-2-butene experiment. For the NO$_3$ radical and 2,3-dimethyl-2-butene only model results are shown. Vertical dashed lines indicate the times when different species where injected. No difference is observed when using the updated MCMv3.3.1 (M0) or a modified version which includes formation of alkoxy radical from the reaction between nitrate-RO$_2$ and HO$_2$ radicals (M1).

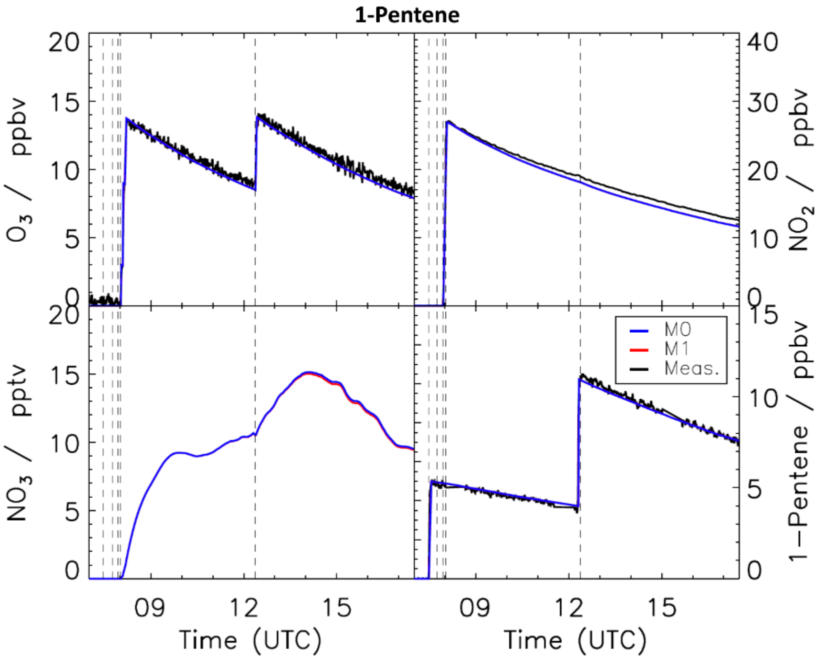

Figure S15: Comparison of modelled and measured trace gases for the 1-pentene experiment. For the NO$_3$ radical only model results are shown. Vertical dashed lines indicate the times when different species where injected. No difference is observed when using the updated MCMv3.3.1 (M0) or a modified version which includes formation of alkoxy radical from the reaction between nitrate-RO$_2$ and HO$_2$ radicals (M1).

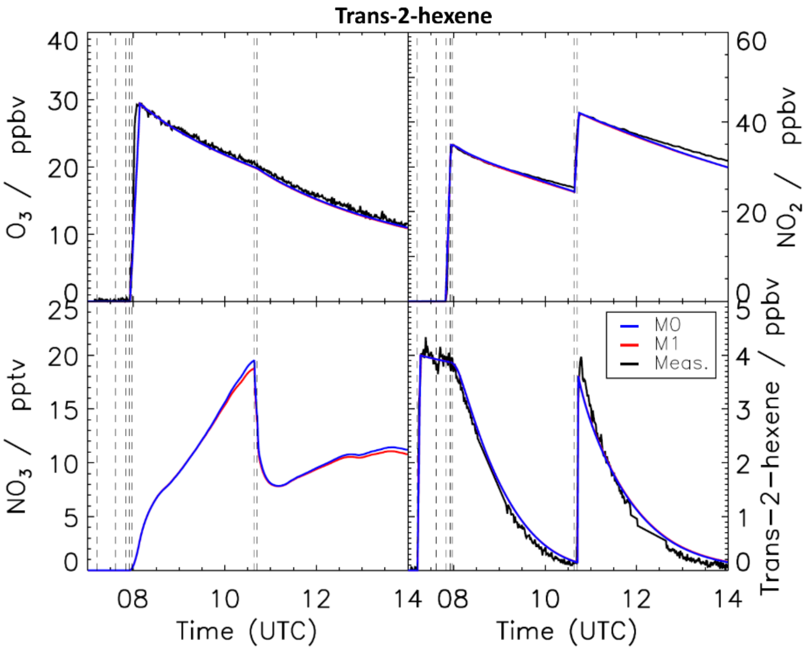

Figure S16: Comparison of modelled and measured trace gases for the trans-2-hexene experiment. For the NO_3 radical only model results are shown. Vertical dashed lines indicate the times when different species where injected. No difference is observed when using the updated MCMv3.3.1 (M0) or a modified version which includes formation of alkoxy radical from the reaction between nitrate-RO_2 and HO_2 radicals (M1).

G. OH yields for β-nitrate-RO_2 + HO_2 reactions

The HO_2 measurements suggest an additional source of HOx in the model. We enhanced the base M0 model with an extra channel in the β-nitrate-RO_2 + HO_2 reaction forming OH + β-nitrate-RO (model M1). The yields of OH are an adjustable parameter in the models. It should be noted that these optimized yields are subject to uncertainty in other chemistry in the model, as over/underestimating OH or HO_2 yields in other reactions reflect directly on the OH yield in the RO_2+HO_2 reaction required to match the observed HO_2. The derived yields are given in the table below, as are the scarce literature data.

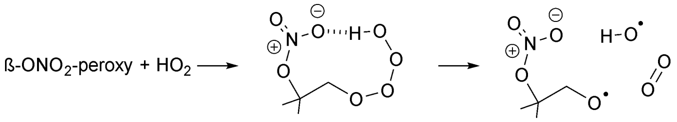

Table S3: **Yields of alkoxy radical plus OH for the reaction between nitrate RO_2 and HO_2 radicals as used within this study in M1.**

Parent compound	Yield	Reference
Ethene	not sensitive	This work
Propene	0.50	This work
Cis-2-butene	0.45	This work
TM2,3-dimethyl-2-butene	0.65	This work
1-Pentene	0.15	This work
Trans-2-hexene	0.40	This work
Isoprene	0.35-0.58	Kwan et al. [49]
	0.22-0.25	Schwantes et al. [50]
	0.5	Wennberg et al. [51]
α-pinene	0.55-0.85	Kurtén et al.[52]

H. Model to measurement HO_2 radical comparison

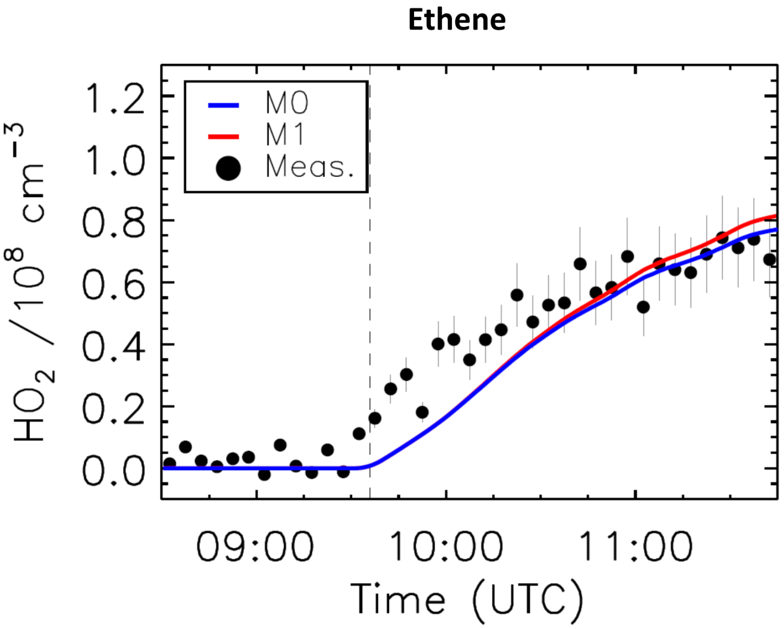
Ethene

Figure S17: Comparison of modelled and measured HO_2 radicals for the ethene experiment. Due to the small CO concentration, no difference is observed when using the updated MCMv3.3.1 (M0) or a modified version which includes formation of alkoxy radical from the reaction between nitrate-RO_2 and HO_2 radicals (M1).

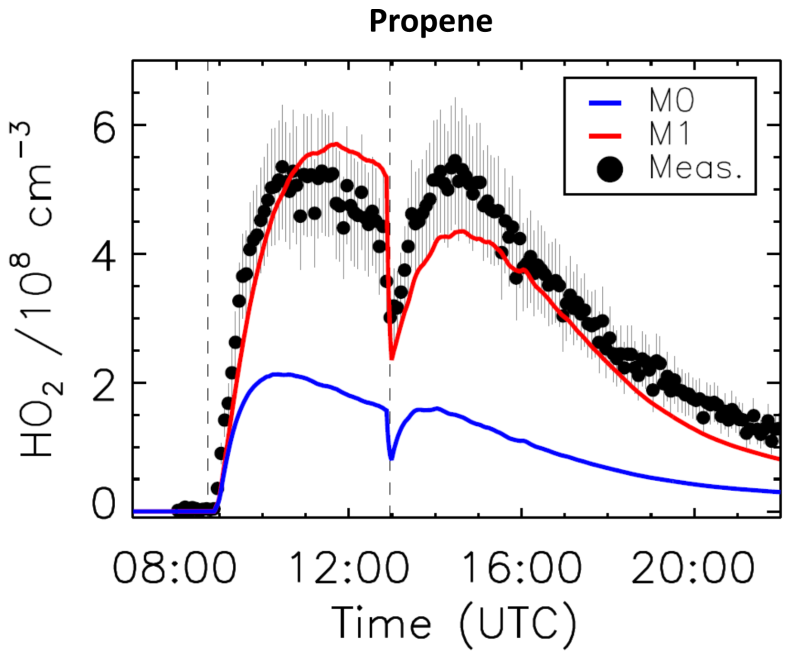
Propene

Figure S18: Comparison of modelled and measured HO_2 radicals for the propene experiment. An increase by almost a factor of two is observed when using a modified version of M0 which includes formation of alkoxy radical from the reaction between nitrate-RO_2 and HO_2 radicals (M1).

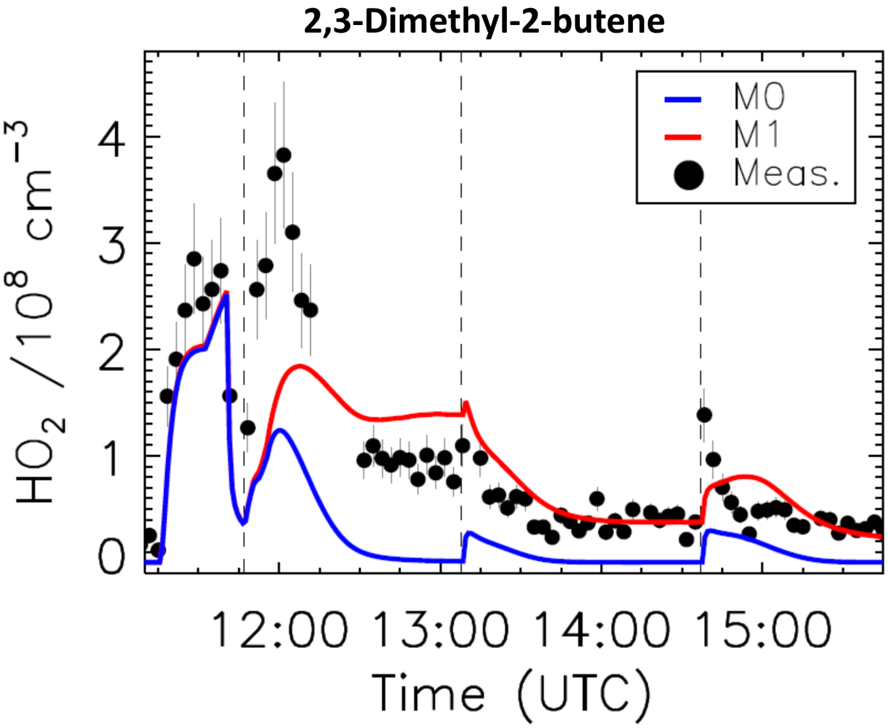

Figure S19: Comparison of modelled and measured HO_2 radicals for the 2,3-dimethyl-2-butene experiment. An increase by almost a factor of two is observed when using a modified version of M0 which includes formation of alkoxy radical from the reaction between nitrate-RO_2 and HO_2 radicals (M1).

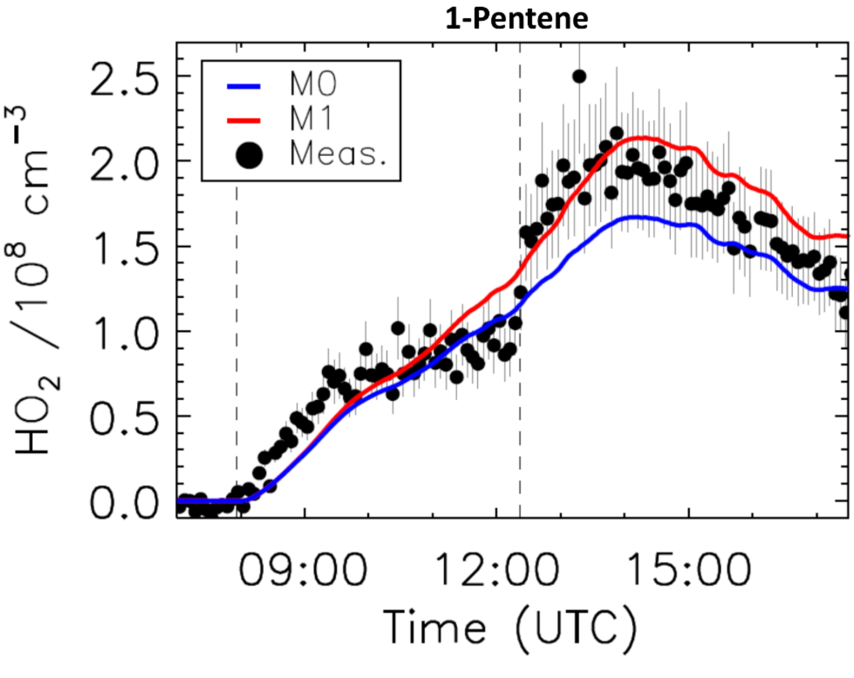

Figure S20: Comparison of modelled and measured HO_2 radicals for the 1-pentene experiment. A better agreement can be observed for the second 1-pentene injection (dominated by NO_3 radical chemistry) when using a modified version of M0 which includes formation of alkoxy radical from the reaction between nitrate-RO_2 and HO_2 radicals (M1).

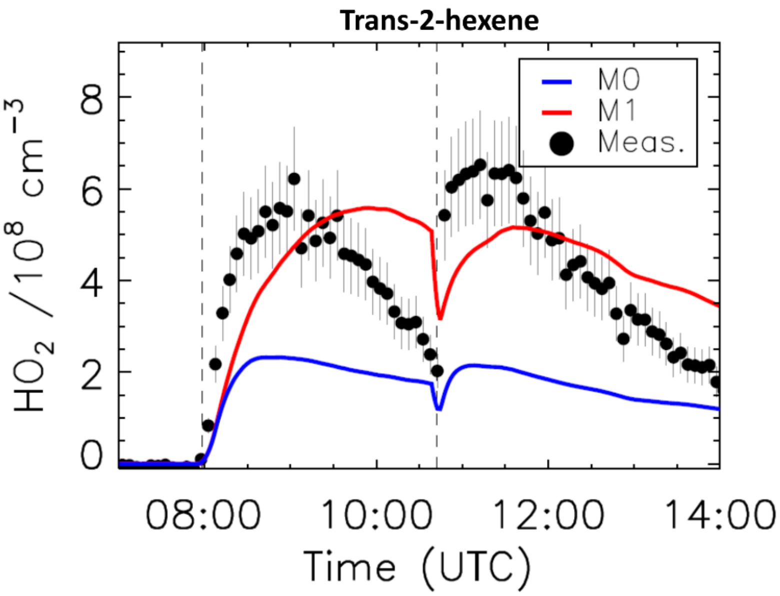

Figure S21: Comparison of modelled and measured HO_2 radicals for the trans-2-hexene experiment. An increase by almost a factor of two is observed when using a modified version of M0 which includes formation of alkoxy radical from the reaction between nitrate-RO_2 and HO_2 radicals (M1).

I. Instrumentation details

Table S4: **Instrumentation for radical and trace-gas quantification during the NO_3 experiments.**

	Technique	Time resolution	1σ precision	1σ accuracy
OH	LIF	47 s	0.3×10^{6} cm^{-3}	18%
HO_2	LIF	47 s	0.5×10^{7} cm^{-3}	18%
RO_2	LIF	47 s	1.0×10^{7} cm^{-3}	18%
k_{OH}	Laser-photolysis + LIF	180 s	0.3 s^{-1}	10%
NO	Chemiluminescence	180 s	4 pptv	5%
NO_2	Chemiluminescence	180 s	2 pptv	5%
O_3	UV-absorption	10 s	1 ppbv	5%
Acetone	PTR-TOF-MS	30 s	> 15 pptv	< 14%
CO	CRDS	60 s	1.5 ppbv	1%

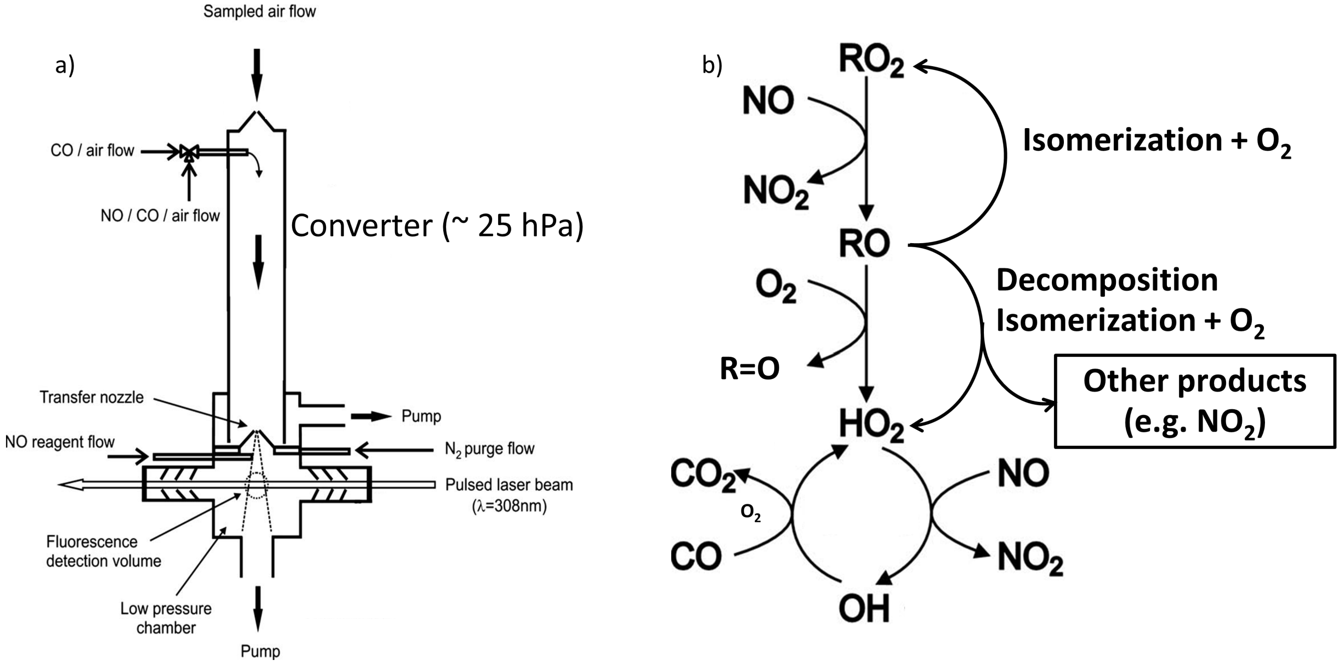

Figure S22: (a) Schematic of the ROxLIF converter and LIF fluorescence cell, updated from Fuchs et al.,[53] and (b) the relevant chemical reactions

J. RO_2 conversion efficiencies using Yeh et al. chemistry

Table S5: **RO_2-specific relative conversion efficiency using alkoxy decomposition rate coefficients from Yeh et al.[53]**

Nitrate-RO_2	**298 K**
Reference RO_2 ($CH_3OO^\bullet$)	1.0
1-ONO_2-2-propylperoxy	3×10^{-3}
2-ONO_2-1-propylperoxy	1.4×10^{-3}
1-ONO_2-2-pentylperoxy	0.25
2-ONO_2-1-pentylperoxy	0.25
2-ONO_2-3-hexylperoxy	0.25
3-ONO_2-2-hexylperoxy	0.25

K. Raw quantum chemical data

The raw quantum chemical data is provided in a separate text file. It contains, for all structures and conformers, the potential energy and geometries at the M06-2X/aug-cc-pVTZ level of theory, as well as the rotational constants, vibrational frequencies, and ZPE corrections. For the lowest conformer(s) of each structure, the potential energy at the CCSD(T)/aug-cc-pVTZ level of theory is also provided, as well as at a few other levels of theory obtained in the course of the CCSD(T) calculations. T1 diagnostics are given. The data also shows the relative energy of all the conformers of a particular structure, and their contribution to the Boltzmann equilibrium population at 298 K.

L. References

1 J.-G. Chang, H.-T. Chen, S. Xu and M. C. Lin, Computational study on the kinetics and mechanisms for the unimolecular decomposition of formic and oxalic Acids, *J. Phys. Chem. A*, 2007, **111**, 6789–6797.

2 H.-T. Chen, J.-G. Chang and H.-L. Chen, A computational study on the decomposition of formic acid catalyzed by $(H_2O)_x$, x=0-3: Comparison of the gas-phase and aqueous-phase results, *J. Phys. Chem. A*, 2008, **112**, 8093–8099.

3 R. M. Vichietti, R. F. Keidel Spada, A. B. Ferreira da Silva, F. B. Correto Machado and R. L. Andrade Haiduke, Accurate Calculations of Rate Constants for the Forward and Reverse H_2O + CO ↔ HCOOH Reactions, *Chemistryselect*, 2017, **2**, 7267–7272.

4 J. Peltola, P. Seal, A. Inkila and A. Eskola, Time-resolved, broadband UV-absorption spectrometry measurements of Criegee intermediate kinetics using a new photolytic precursor: unimolecular decomposition of CH2OO and its reaction with formic acid, *Phys. Chem. Chem. Phys.*, 2020, **22**, 11797–11808.

5 T.-N. Nguyen, R. Putikam and M. C. Lin, A novel and facile decay path of Criegee intermediates by intramolecular insertion reactions via roaming transition states, *J. Chem. Phys.*, 2015, **142**, 124312.

6 T. L. Nguyen, H. Lee, D. A. Matthews, M. C. McCarthy and J. F. Stanton, Stabilization of the Simplest Criegee Intermediate from the Reaction between Ozone and Ethylene: A High Level Quantum Chemical and Kinetic Analysis of Ozonolysis, *J. Phys. Chem. A*, 2015, **119**, 5524–5533.

7 B. Ruscic and D. H. Bross, Active Thermochemical Tables (ATcT) values based on ver. 1.122g of the Thermochemical Network (2019); available at ATcT.anl.gov, http://atct.anl.gov/.

8 D. Stone, K. Au, S. Sime, D. J. Medeiros, M. Blitz, P. W. Seakins, Z. Decker and L. Sheps, Unimolecular decomposition kinetics of the stabilised Criegee intermediates CH_2OO and CD_2OO, *Phys. Chem. Chem. Phys.*, 2018, **20**, 24940–24954.

9 M. Pfeifle, Y.-T. Ma, A. W. Jasper, L. B. Harding, W. L. Hase and S. J. Klippenstein, Nascent energy distribution of the Criegee intermediate CH_2OO from direct dynamics calculations of primary ozonide dissociation, *J. Chem. Phys.*, 2018, **148**, 174306.

10 L. Vereecken and J. Peeters, Decomposition of substituted alkoxy radicals—part I: a generalized structure–activity relationship for reaction barrier heights, *Phys. Chem. Chem. Phys.*, 2009, **11**, 9062–9074.

11 IUPAC Subcommittee on Atmospheric Chemical Kinetic Data Evaluation, *Evaluated Kinetic Data*, IUPAC, 2017.

12 L. Vereecken, A. Novelli and D. Taraborrelli, Unimolecular decay strongly limits concentration of Criegee intermediates in the atmosphere, *Phys. Chem. Chem. Phys.*, 2017, **19**, 31599–31612.

13 O. Horie and G. K. Moortgat, Decomposition Pathways of the Excited Criegee Intermediates in the Ozonolysis of Simple Alkenes, *Atmos. Environ.*, 1991, **25**, 1881–1896.

14 M. J. Newland, B. S. Nelson, A. Munoz, M. Rodenas, T. Vera, J. Tarrega and A. R. Rickard, Trends in stabilisation of Criegee intermediates from alkene ozonolysis, *Phys. Chem. Chem. Phys.*, 2020, **22**, 13698–13706.

15 S. Hatakeyama, H. Kobayashi and H. Akimoto, Gas-phase oxidation of sulfur dioxide in the ozone-olefin reactions, *J. Phys. Chem.*, 1984, **88**, 4736–4739.

16 A. R. Rickard, D. Johnson, C. D. McGill and G. Marston, OH yields in the gas-phase reactions of ozone with alkenes, *J. Phys. Chem. A*, 1999, **103**, 7656–7664.

17 Y. Fang, F. Liu, V. P. Barber, S. J. Klippenstein, A. B. McCoy and M. I. Lester, Communication: Real time observation of unimolecular decay of Criegee intermediates to OH radical products, *J. Chem. Phys.*, 2016, **144**, 061102.

18 Y. Fang, F. Liu, V. P. Barber, S. J. Klippenstein, A. B. McCoy and M. I. Lester, Deep tunneling in the unimolecular decay of CH_3CHOO Criegee intermediates to OH radical products, *J. Chem. Phys.*, 2016, **145**, 234308.

19 B. Long, J. L. Bao and D. G. Truhlar, Atmospheric Chemistry of Criegee Intermediates. Unimolecular Reactions and Reactions with Water, *J. Am. Chem. Soc.*, 2016, **138**, 14409–14422.

20 T. L. Nguyen, L. McCaslin, M. C. McCarthy and J. F. Stanton, Communication: Thermal unimolecular decomposition of syn-CH_3CHOO: A kinetic study, *J. Chem. Phys.*, 2016, **145**, 131102.

21 C. D. McGill, A. R. Rickard, D. Johnson and G. Marston, Product yields in the reactions of ozone with Z-but-2-ene, E-but-2-ene and 2-methylbut-2-ene, *Chemosphere*, 1999, **38**, 1205–1212.

22 W. C. D. Rathman, T. A. Claxton, A. R. Rickard and G. Marston, A theoretical investigation of OH formation in the gas-phase ozonolysis of E-but-2-ene and Z-but-2-ene, *Phys. Chem. Chem. Phys.*, 1999, **1**, 3981–3985.

23 G. E. Orzechowska and S. E. Paulson, Photochemical sources of organic acids. 1. Reaction of ozone with isoprene, propene, and 2-butenes under dry and humid conditions using SPME, *J. Phys. Chem. A*, 2005, **109**, 5358–5365.

24 S. C. Moldoveanu, in *Techniques and Instrumentation in Analytical Chemistry*, Elsevier, 2010, vol. 28, pp. 471–526.

25 P. Ruelle, Ab initio quantum-chemical study of the unimolecular pyrolysis mechanisms of acetic acid, *Chem. Phys.*, 1986, **110**, 263–274.

26 A. M. Verma and N. Kishore, Kinetics of Decomposition Reactions of Acetic Acid Using DFT Approach, *Open Chem. Eng. J.*, 2018, **12**, 14–23.

27 L. Zhang, L. Yao, Q. Li, G. Wang and S. H. Lin, Anharmonic effect of the unimolecular dissociation of CH_3COOH, *Mol. Phys.*, 2014, **112**, 2853–2871.

28 T. Berndt, T. Jokinen, R. L. Mauldin, T. Petäjä, H. Herrmann, H. Junninen, P. Paasonen, D. R. Worsnop and M. Sipilä, Gas-Phase Ozonolysis of Selected Olefins: The Yield of Stabilized Criegee Intermediate and the Reactivity toward SO_2, *J. Phys. Chem. Lett.*, 2012, **3**, 2892–2896.

29 M. Campos-Pineda and J. Zhang, Product yields of stabilized Criegee intermediates in the ozonolysis reactions of cis-2-butene, 2-methyl-2-butene, cyclopentene, and cyclohexene, *Sci. China-Chem.*, 2018, **61**, 850–856.

30 T. A. H. Burd, X. Shan and D. C. Clary, Catalysis and tunnelling in the unimolecular decay of Criegee intermediates, *Phys. Chem. Chem. Phys.*, 2018, DOI: 10.1039/C8CP05021J.

31 R. Chhantyal-Pun, O. Welz, J. D. Savee, A. J. Eskola, E. P. F. Lee, L. Blacker, H. R. Hill, M. Ashcroft, M. A. H. H. Khan, G. C. Lloyd-Jones, L. A. Evans, B. Rotavera, H. Huang, D. L. Osborn, D. K. W. Mok, J. M. Dyke, D. E. Shallcross, C. J. Percival, A. J. Orr-Ewing and C. A. Taatjes, Direct Measurements of Unimolecular and Bimolecular Reaction Kinetics of the Criegee Intermediate $(CH_3)_2COO$, *J. Phys. Chem. A*, 2017, **121**, 4–15.

32 Y. Fang, V. P. Barber, S. J. Klippenstein, A. B. Mccoy and M. I. Lester, Tunneling effects in the unimolecular decay of $(CH_3)_2COO$ Criegee intermediates to OH radical products, *J. Chem. Phys.*, 2017, **146**, 134307.

33 G. E. Orzechowska, H. T. Nguyen and S. E. Paulson, Photochemical sources of organic acids. 2. Formation of C_5-C_9 carboxylic acids from alkene ozonolysis under dry and humid conditions, *J. Phys. Chem. A*, 2005, **109**, 5366–5375.

34 L. Vereecken and H. M. T. Nguyen, Theoretical study on the reaction of carbonyl oxide with nitrogen dioxide: CH_2OO + NO_2, *Int. J. Chem. Kinet.*, 2017, **49**, 752–760.

35 R. L. Caravan, M. A. H. Khan, B. Rotavera, E. Papajak, I. O. Antonov, M.-W. Chen, K. Au, W. Chao, D. L. Osborn, J. J.-M. Lin, C. J. Percival, D. E. Shallcross and C. A. Taatjes, Products of Criegee intermediate reactions with NO_2: experimental measurements and tropospheric implications, *Faraday Discuss.*, 2017, **200**, 313–330.

36 L. Vereecken, A. R. Rickard, M. J. Newland and W. J. Bloss, Theoretical study of the reactions of Criegee intermediates with ozone, alkylhydroperoxides, and carbon monoxide, *Phys. Chem. Chem. Phys.*, 2015, **17**, 23847–23858.

37 A. Kumar and P. Kumar, CO_2 as an auto-catalyst for the oxidation of CO by a Criegee intermediate (CH_2OO), *Phys. Chem. Chem. Phys.*, 2020, **22**, 6975–6983.

38 M. Kumar, D. H. Busch, B. Subramaniam and W. H. Thompson, The Criegee Intermediate Reaction with CO. Mechanism, Barriers, Conformer-Dependence, and Implications for Ozonolysis Chemistry, *J. Phys. Chem. A*, 2014, **118**, 1887–1894.

39 M. E. Jenkin, R. Valorso, B. Aumont and A. R. Rickard, Estimation of rate coefficients and branching ratios for reactions of organic peroxy radicals for use in automated mechanism construction, *Atmospheric Chem. Phys.*, 2019, **19**, 7691–7717.

40 D. Johnson and G. Marston, The gas-phase ozonolysis of unsaturated volatile organic compounds in the troposphere, *Chem. Soc. Rev.*, 2008, **37**, 699–716.

41 L. Vereecken and J. S. Francisco, Theoretical studies of atmospheric reaction mechanisms in the troposphere, *Chem. Soc. Rev.*, 2012, **41**, 6259–6293.

42 L. Vereecken and B. Nozière, H migration in peroxy radicals under atmospheric conditions, *Atmospheric Chem. Phys.*, 2020, **20**, 7429–7458.

43 H. C. Knap and S. Jørgensen, Rapid Hydrogen Shift Reactions in Acyl Peroxy Radicals, *J. Phys. Chem. A*, 2017, **121**, 1470–1479.

44 L. Vereecken and J. Peeters, A structure–activity relationship for the rate coefficient of H-migration in substituted alkoxy radicals, *Phys. Chem. Chem. Phys.*, 2010, **12**, 12608–12620.

45 A. Novelli, L. Vereecken, B. Bohn, H.-P. Dorn, G. I. Gkatzelis, A. Hofzumahaus, F. Holland, D. Reimer, F. Rohrer, S. Rosanka, D. Taraborrelli, R. Tillmann, R. Wegener, Z. Yu, A. Kiendler-Scharr, A. Wahner and H. Fuchs, Importance of isomerization reactions for the OH radical regeneration from the photo-oxidation of isoprene investigated in the atmospheric simulation chamber SAPHIR, *Atmospheric Chem. Phys.*, 2020, **20**, 3333–3355.

46 O. M. Anglada, R. Crehuet and J. S. Francisco, The Stability of alpha-Hydroperoxyalkyl Radicals, *Chem.- Eur. J.*, 2016, **22**, 18092–18100.

47 L. Vereecken, Computational study of the stability of α-nitroxy-substituted alkyl radicals, *Chem. Phys. Lett.*, 2008, **466**, 127–130.

48 L. Vereecken, T. L. Nguyen, I. Hermans and J. Peeters, Computational study of the stability of α-hydroperoxyl- or α-alkylperoxyl substituted alkyl radicals, *Chem. Phys. Lett.*, 2004, **393**, 432–436.

49 A. J. Kwan, A. W. H. Chan, N. L. Ng, H. G. Kjaergaard, J. H. Seinfeld and P. O. Wennberg, Peroxy radical chemistry and OH radical production during the NO_3-initiated oxidation of isoprene, *Atmospheric Chem. Phys.*, 2012, **12**, 7499–7515.

50 R. H. Schwantes, A. P. Teng, T. B. Nguyen, M. M. Coggon, J. D. Crounse, J. M. St Clair, X. Zhang, K. A. Schilling, J. H. Seinfeld and P. O. Wennberg, Isoprene NO_3 Oxidation Products from the RO_2 + HO_2 Pathway, *J. Phys. Chem. A*, 2015, **119**, 10158–10171.

51 P. O. Wennberg, K. H. Bates, J. D. Crounse, L. G. Dodson, R. C. McVay, L. A. Mertens, T. B. Nguyen, E. Praske, R. H. Schwantes, M. D. Smarte, J. M. St Clair, A. P. Teng, X. Zhang and J. H. Seinfeld, Gas-Phase Reactions of Isoprene and Its Major Oxidation Products, *Chem. Rev.*, 2018, **118**, 3337–3390.

52 T. Kurtén, K. H. Møller, T. B. Nguyen, R. H. Schwantes, P. K. Misztal, L. Su, P. O. Wennberg, J. L. Fry and H. G. Kjaergaard, Alkoxy Radical Bond Scissions Explain the Anomalously Low Secondary Organic Aerosol and Organonitrate Yields From alpha-Pinene + NO3, *J. Phys. Chem. Lett.*, 2017, **8**, 2826–2834.

53 H. Fuchs, F. Holland and A. Hofzumahaus, Measurement of tropospheric RO_2 and HO_2 radicals by a laser-induced fluorescence instrument, *Rev. Sci. Instrum.*, 2008, **79**, 084104.

54 G. K. Yeh, M. S. Claflin and P. J. Ziemann, Products and Mechanism of the Reaction of 1-Pentadecene with NO_3 Radicals and the Effect of a -ONO_2 Group on Alkoxy Radical Decomposition, *J. Phys. Chem. A*, 2015, **119**, 10684–10696.